Biological Conservation 217 (2018) 289–310

Contents lists available at ScienceDirect

Biological Conservation

journal homepage: www.elsevier.com/locate/biocon

Mapped aboveground carbon stocks to advance forest conservation and recovery in Malaysian Borneo

Gregory P. Asner[a,*], Philip G. Brodrick[a], Christopher Philipson[b], Nicolas R. Vaughn[a], Roberta E. Martin[a], David E. Knapp[a], Joseph Heckler[a], Luke J. Evans[a], Tommaso Jucker[c], Benoit Goossens[d], Danica J. Stark[d], Glen Reynolds[e], Robert Ong[f], Nathan Renneboog[g], Fred Kugan[f], David A. Coomes[h]

[a] Department of Global Ecology, Carnegie Institution for Science, Stanford, CA 94305, USA
[b] Department of Environmental Systems Science, ETH Zürich, Zürich, Switzerland
[c] CSIRO Land and Water Flagship, Wembley, Australia
[d] Danau Girang Field Centre, Sabah, Malaysia, Sabah Wildlife Department, Sabah Malaysia, Cardiff University, Cardiff, UK
[e] South East Asia Rainforest Research Partnership, Sabah, Malaysia
[f] Sabah Forestry Department, Sandakan, Malaysia
[g] Permian Global, London, UK
[h] Department of Plant Sciences, University of Cambridge, Cambridge, UK

ARTICLE INFO

Keywords:
Borneo
Carbon conservation
Carnegie airborne observatory
Deforestation
Land use history
Forest conservation
Sabah
Selective logging

ABSTRACT

Forest carbon stocks in rapidly developing tropical regions are highly heterogeneous, which challenges efforts to develop spatially-explicit conservation actions. In addition to field-based biodiversity information, mapping of carbon stocks can greatly accelerate the identification, protection and recovery of forests deemed to be of high conservation value (HCV). We combined airborne Light Detection and Ranging (LiDAR) with satellite imaging and other geospatial data to map forest aboveground carbon density at 30 m (0.09 ha) resolution throughout the Malaysian state of Sabah on the island of Borneo. We used the mapping results to assess how carbon stocks vary spatially based on forest use, deforestation, regrowth, and current forest protections. We found that unlogged, intact forests contain aboveground carbon densities averaging over 200 Mg C ha^{-1}, with peaks of 500 Mg C ha^{-1}. Critically, more than 40% of the highest carbon stock forests were discovered outside of areas designated for maximum protection. Previously logged forests have suppressed, but still high, carbon densities of 60–140 Mg C ha^{-1}. Our mapped distributions of forest carbon stock suggest that the state of Sabah could double its total aboveground carbon storage if previously logged forests are allowed to recover in the future. Our results guide ongoing efforts to identify HCV forests and to determine new areas for forest protection in Borneo.

1. Introduction

Forest carbon stock is a time-integrated expression of numerous processes ranging from plant growth and mortality to natural disturbance and human land use. The spatial distribution of aboveground carbon density (ACD), measured in units of megagrams (Mg = metric tons) of carbon (C) per hectare (ha), is therefore affected by spatially variable factors that control growth and mortality, such as climate and biodiversity, and by the rate, spatial pattern and severity of disturbances such as storms, logging, and fire (Brown and Lugo, 1982; Houghton, 2000; Kasischke et al., 1995). Mapping and monitoring of ACD has become increasingly routine (Asner et al., 2012a; Zolkos et al., 2013), and now offers to accelerate efforts to conserve forests in the context of climate change mitigation by identifying areas of high-biomass, old growth canopies and/or areas deemed ecologically viable for recovery (Lindenmayer et al., 2013; Smith et al., 2000; UNFCCC, 2009). Carbon stock mapping may also complement other types of mapping for decision-making, such as for biodiversity protection, although high carbon stocks are not always correlated with high species diversity (Sullivan et al., 2017).

Forest carbon stocks of the 7.25 million ha State of Sabah in Malaysian Borneo are a key case-in-point. Like much of Malaysia and Indonesia, Sabah has a centennial history of widespread forest exploitation via selective logging for timber (Jomo et al., 2004; Pinard et al., 1996), which has more recently been followed by clear-cutting for oil palm and timber plantation development (Bryan et al., 2013).

* Corresponding author.
E-mail address: gpa@carnegiescience.edu (G.P. Asner).

https://doi.org/10.1016/j.biocon.2017.10.020
Received 16 June 2017; Received in revised form 5 October 2017; Accepted 18 October 2017
Available online 22 November 2017

Today, remaining natural forests cover about 59% of Sabah, and most have been heavily but variably logged. Many of these forests are also actively being assessed in a process of ongoing land reallocation either for protection or other uses, but with an ongoing risk of the elimination of forest reserves to develop agricultural plantations. Like many developing tropical forest regions, Sabah's forest carbon landscapes are extremely heterogeneous, with ACD levels varying in non-random, nested patterns at local to regional scales. Heavily impacted landscapes such as Sabah have the added complexity of diverse, poorly known forest disturbance histories generated by years of multiple entry logging and post-timber extraction treatment. As a result, the forest carbon mosaic of Sabah cannot be reasonably assessed using ground-based inventory or partial-coverage mapping approaches. A complete, wall-to-wall mapping is required by the state government to identify forests for new conservation action, and for future assessments of management performance. Moreover, a mapping of Sabah's aboveground forest carbon stocks, in addition to biodiversity, has been undertaken with United Nations Development Programme and multiple non-government organizational support to facilitate the selection of high conservation value (HCV) forests for a new large protected area.

Sabah's remaining natural forests, excluding mangroves, cover an area of about 3.7 million ha and are legally allocated to one of seven forest reserve classes, or are designated as parks or wildlife sanctuaries and conservation areas (Fig. A1). Class I, VI, and VII forest reserves, parks and the wildlife designations are considered the most protected in terms of forest carbon stocks and biological diversity. Class II, III, and IV reserves are under highly variable management, and as a result, they harbor widely varying degrees of carbon and biodiversity conservation. However, independent of current designation, nearly all of these forests previously underwent selective logging, with only a few exceptions such as Maliau Basin, Imbak Canyon, and parts of Kinabalu mountain, the Crocker Range and Danum Valley (Bryan et al., 2013; Gaveau et al., 2014). Gaveau et al. (2016) provided the most current estimate of previously deforested land in Borneo, reporting > 1.86 million ha of deforestation between 1973 and 2015 in Sabah alone. Their study did not resolve forest carbon stocks on previously deforested lands or in regrowing forests.

Today, the Sabah government seeks to increase protected forests from about 1.8 to 2.2 million ha, representing an increase from about 25% to 30% of the state. A process is now underway to identify candidate forests for protection, an effort based on ecological, social, economic and political factors. From an ecological standpoint, areas best suited for increased protection are those that: (i) store the most carbon currently and/or which could do so in the future, and (ii) that harbor the highest biodiversity including endemic and highly endangered species. In this context, we sought to develop the first high-resolution map of forest aboveground carbon density, as a contribution to advance a portion of the conservation planning activity for the Sabah State government.

Here we report on forest ACD throughout Sabah, along with an analysis of how ACD varies spatially based on forest use, deforestation, regrowth, and current forest protections. We combine airborne Light Detection and Ranging (LiDAR) sampling with wall-to-wall satellite imaging and other geospatial data to estimate forest ACD at 30 m (0.09 ha) resolution. Our approach provides a spatially-explicit understanding of aboveground carbon stocks by land allocation throughout Sabah, and facilitates rapid identification of candidate areas for forest protection.

2. Methods

Generating the wall-to-wall map of ACD throughout the State of Sabah required the integration of airborne data and regional modeling techniques. A flight campaign was undertaken to acquire LiDAR data, which were subsequently processed and converted into ACD estimates via statistical modeling. To extend the ACD estimates from the flight data to the entire state, we compiled a wide array of environmental data and used a deep learning model to upscale the flight data to wall-to-wall coverage. Finally, we estimated spatially-explicit uncertainty and determined the relative influence of different environmental variables on ACD distribution. We describe each of these steps in the following sections.

2.1. Airborne data collection

We collected LiDAR data using the Carnegie Airborne Observatory-3 (CAO; Asner et al., 2012b) throughout Sabah in April 2016. The airborne sampling was designed to cover large portions of high-priority forested research and calibration landscapes, plus all forested landscapes deemed valuable for statewide mapping based on environmental heterogeneity. In total, 2.1 million ha of LiDAR data were collected, equivalent to approximately 29% of Sabah, and the sampling was distributed spatially based on a geostatistical modeling technique (Fig. A2).

During data collection, the field-of-view of the LiDAR was set to 38°, and we trimmed 2° from each side during data processing to remove edge effects, leaving a final field of view of 34°. We used a LiDAR pulse frequency of 200 kHz (combined from two channels), a scan frequency of 24 Hz, and the aircraft speed was maintained at or below 130 knots. These settings were selected to reduce variation in the along-track and across-track pulse spacing, and to achieve a minimum pulse density of 1.14 pulses m^{-2} (or 4.5 returns m^{-2}). The final trajectories from each flight during the campaign had an estimated precision continually < 7 cm. The average root mean squared error (RMSE) of point position errors in the refined point clouds was 9.4 cm.

The geostatistical sampling technique was designed to maximize the coverage and cost efficiency of the airborne LiDAR sampling in support of spatially-continuous map generation. The technique uses a computational machine learning algorithm to link the high-resolution data collected by the CAO to statewide satellite and terrain data, hereafter referred to as the 'environmental data', as described later. These environmental data were prepared at 30 m (0.09 ha) spatial resolution, and incorporated a diverse array of satellite reflectance and radar products as well as elevation, slope, aspect, and related topographic data, described later.

Collecting sufficient airborne LiDAR data for the statewide mapping required near real-time analysis during flight operations to determine if the quantity and variety of environments had been adequately sampled with the CAO. Two criteria were used to make this determination: (i) the CAO data must be collected in a geographically dispersed pattern throughout Sabah, and (ii) the CAO data collected must encompass the variation in the environmental data covering the State of Sabah. These two criteria were addressed simultaneously by partitioning Sabah into 150 grid cells of 25 km × 25 km in size. By collecting enough airborne data such that a model of the environmental variation could be produced for each of these grid cells, we ensured that our sampling satisfied the first criterion. The use of the geographically dispersed grid cells ensured that the second criterion was met when the variation defined by the environmental data was sufficiently modeled within each grid cell as determined by precision saturation of the sampling statistics. Satisfying these two criteria indicated that collecting additional aircraft data would provide little additional value in the generation of a statewide carbon map.

Meeting the first criterion was straightforward: the CAO data were collected within each grid cell. Addressing the second criterion required analysis during the flight campaign. To track our progress towards sufficient modeling of the environmental variation, a metric was used to track changes in the precision of the statistical model applied to each grid cell. We generated statistical models of vegetation canopy height derived from canopy height measurements made with the CAO LiDAR. Following each flight, a model was generated by combining LiDAR canopy height estimates with the environmental data within each grid

cell. These models were generated using the Random Forest Machine Learning (RFML) algorithm (Breiman, 2001), selected for its computational speed needed for regional modeling during airborne data collection. RFML uses an ensemble of decision trees to quantify the relationship between environmental data within each grid cell and the LiDAR data collected by the CAO. The cloud-masked, LiDAR-derived canopy height observations were coarsened from 1 m to 30 m resolution to match the resolution of the environmental dataset.

During flight operations, each grid cell was updated with the increasing coverage of CAO data, which subsequently updated the grid-based RFML models (Fig. A3a). Each grid cell model predicted the tree heights over the entire cell, and the root mean squared error (RMSE) between successive model predictions was determined. When the change in the RMSE decayed to a constant, we considered the grid cell to be 'data saturated,' and collecting additional data within that cell became a low priority. The asymptote of data values was detected by tracking the change in model performance as LiDAR data coverage was increased in the grid cell. To detect this asymptote, we used thresholds of 5 cm and 15 cm in the rate of change of successive models of canopy height as LiDAR data coverage was increased within the grid cell. The grid cell was said to be fully data saturated with LiDAR data if the 5 cm threshold was reached. The grid cell was said to be nearly data saturated if the 15 cm threshold is reached. This technique to maximize model precision in each grid cell, coupled with spatially diverse sampling across the entire set of 150 grid cells throughout Sabah, ensured that the LiDAR data collection provided a comprehensive sampling of the State.

On a grid-cell basis, our statistical models indicated that an average of 8.3% (standard deviation = 2.3%) of each cell required LiDAR coverage to achieve full geostatistical saturation. Our achieved coverage far exceeded this threshold, with an average 29.5% (standard deviation = 16.5%) of each cell sampled with LiDAR (Fig. A3b). Oversampling was a result of the efficiency of airborne LiDAR data collection during mapping operations, combined with aircraft transits and other flight activities across the region during the campaign.

We emphasize here that our cell-by-cell saturation analysis is highly conservative. After all flying is completed, the grid cell-based calculations are no longer used, and all data are incorporated into a statewide model for each data product generated (e.g., canopy height, aboveground carbon density). The grid cell-based approach used during flight operations ensures enormous data density and spacing across Sabah.

2.2. Data processing

While flights were conducted to avoid as much cloud cover as possible, many areas were still flown above clouded terrain. Cloud cover under the aircraft results in enough noise in the data to interfere with data processing. We eliminated clouds using an automatic algorithm that removes points that deviate significantly from NASA Shuttle Radar Topography Mission (SRTM) elevation. Remaining cloud patches were removed manually from the data through careful and exhaustive examination.

We used the LAStools (rapidlasso, GmbH; Gilching, Germany) suite of computational tools to identify ground points and interpolate ground and upper canopy returns into 2 m resolution maps of bare-earth ground elevation (DEM) and top-of-canopy height above ground (TCH) for each flight line (Fig. A4). We then combined the TCH data from each flight line into a single mosaic. After the 2 m TCH maps are created, we then average pixels together to generate 30 m resolution TCH maps. We also used the 2 m TCH data to calculate the fraction of each 30 m resolution pixel that exceeds 20 m, known as $Cover_{20}$ (Jucker et al., 2017).

2.3. Field calibration to aboveground carbon density

We used a network of field calibration plots comprised of previously measured plots (Coomes et al., 2017), and new plots developed using the CAO field inventory protocol (Asner and Mascaro, 2014). Field plots varied in size from 0.28 ha to 1.0 ha, and each plot had to, at a minimum, provide measurements of live and dead standing tree diameters at breast height (dbh) and canopy height for stems > 10 cm, as well as knowledge of the tree genera present for use in wood density estimation. For each plot, we calculated ACD_{est} using the *BIOMASS* workflow of Réjou-Méchain et al. (2017), which propagates uncertainty in estimated ACD arising from field measurement errors and uncertainty in allometric models. Equations from Asner and Mascaro (2014) were used to estimate aboveground carbon density (ACD_{est}) from LiDAR TCH in meters, with a modification to incorporate canopy cover at 20 m aboveground, also derived from LiDAR data (Jucker et al., 2017). The ACD_{est} calibration was performed in two steps. First, we calculated the residual of a nonlinear fit between TCH and $Cover_{20}$ so that we minimize the influence of collinearity on ACD_{est}, as:

$$Cover_{resid} = Cover_{20} - \frac{1}{1 + e^{12.3529} \times TCH^{-4.1108}}.$$

Next, we used $Cover_{resid}$ and TCH to estimate ACD, as:

$$ACD_{est} = 0.62369 \times TCH^{1.63899}(1 + 1.983 \times Cover_{resid})^{1.081}.$$

Fig. A5 illustrates the application of this equation to all CAO flight data. These equations were calibrated with airborne LiDAR data collected by the CAO and a British research aircraft (Jucker et al., 2017), and represents a robust approach that is applicable across LiDAR platforms.

2.4. Environmental data for regional upscaling

We used a combination of environmental data for the upscaling of the airborne LiDAR to the Sabah statewide level (Figs. A6–A8). Generic spatial distance was modeled in latitude and longitude. Four topographic variables (elevation, slope, aspect and relative elevation) were calculated from NASA Shuttle Radar Topography Mission (SRTM) data. Relative elevation was calculated as the elevation above the nearest water body, providing an index of local topography and hydrology (Asner et al., 2014).

Numerous satellite data sources were investigated and compiled to generate the environmental data used for upscaling the airborne LiDAR to the statewide level. We compiled Landsat-8 surface reflectance images for a one-year period (15 Oct 2015–15 Oct 2016), processed to surface reflectance by the U.S. Geological Survey (Masek et al., 2006), for the State of Sabah. We used the Google Earth Engine (Google, 2015) to mask out clouds, shadow, and water with the *cfmask* band. We then took the median value of each pixel, which further decreased the influence of spurious clouds and shadows. Our initial compositing indicated that there were no unmasked pixels available in 0.05% of the data. In these pixels, we used data from the previous year (15 Oct 2014–15 Oct 2015) processed with the same method. As these instances were rare and only occurred in extremely cloudy areas over dense, intact forests, land-use impacts were less likely to have influenced these pixels. Reflectance bands 3 (green [0.53–0.59 μm]), 4 (red [0.64–0.67 μm]), 5 (near-infrared [0.85–0.88 μm]), 6 (short-wave infrared 1 [1.57–1.65 μm]), and 7 (short-wave infrared 2 [2.11–2.29 μm]) were included in the compositing. We excluded bands 1 and 2 due to atmospheric artifacts including aerosols. The resulting mosaicked Landsat-8 surface reflectance bands 3–7 were spectrally unmixed using the CLASlite forest monitoring approach (Asner et al., 2009). This step generated fractional cover data layers, including photosynthetic vegetation (PV), non-photosynthetic vegetation (NPV), and bare substrate (B), at 30 m resolution, which were used in the upscaling analysis.

Synthetic aperture radar data from the ESA Copernicus Sentinel-1 satellite (Masek et al., 2006) was also used in statewide modeling. We compiled Sentinel-1 images collected using interferometric wide swath

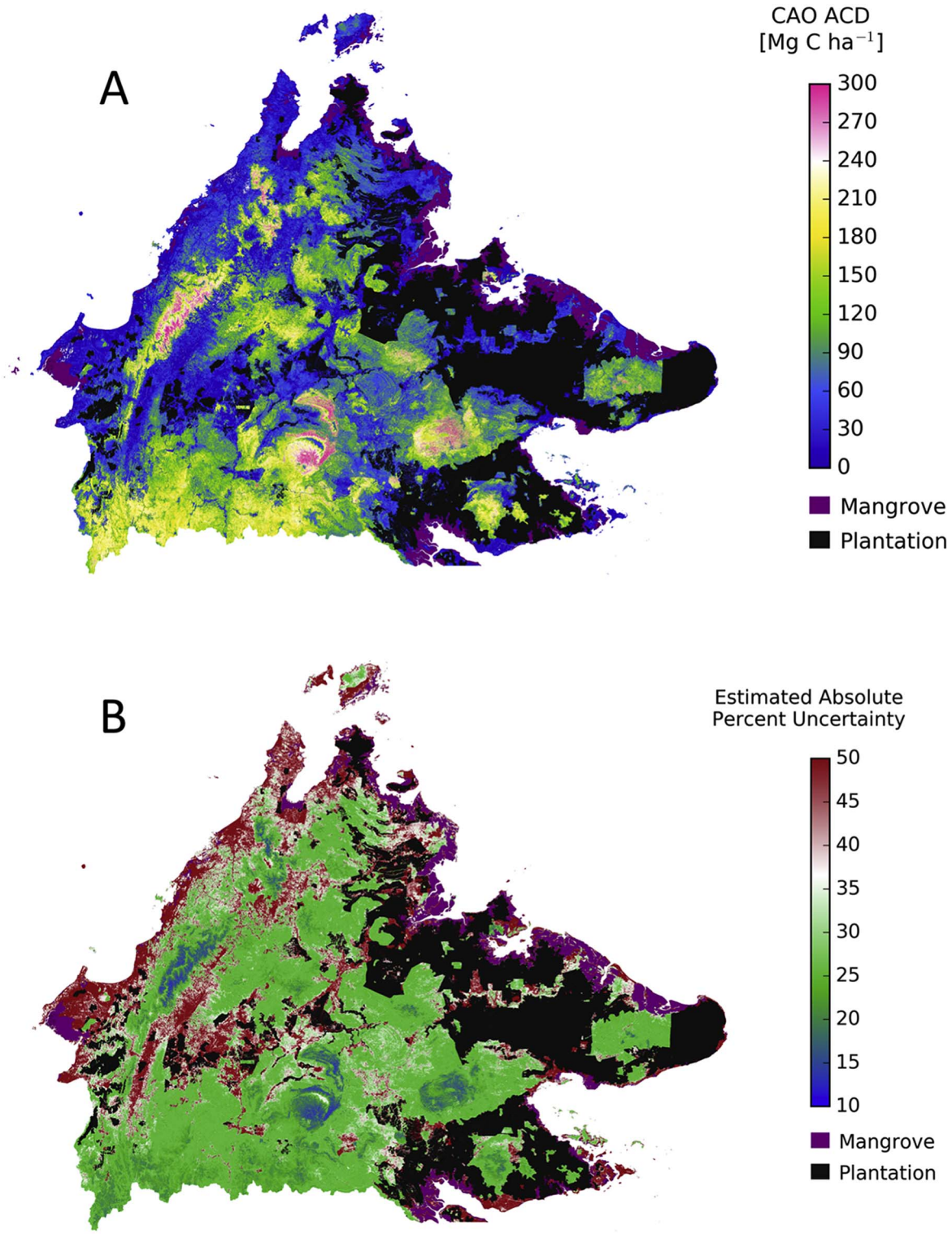

Fig. 1. (A) Aboveground carbon density (ACD) throughout the State of Sabah in Malaysian Borneo, at 30 m (0.09 ha) spatial resolution. Areas covered by mangrove and oil palm plantation are masked out. (B) Estimated absolute uncertainty in units of percent of mapped ACD at 30 m (0.09 ha) resolution.

mode at 10 m ground-level resolution between the dates of 1 Feb and 1 July 2016 using the Google Earth Engine (Google, 2015). We then took the median value of each pixel over that period from with the VH and VV polarizations. Both of these polarizations were included in the upscaling analysis.

2.5. Upscaling from airborne LiDAR samples

We used a supervised machine learning model to upscale airborne LiDAR-derived ACD estimates averaged at 30 m resolution to the suite of environmental data in order to generate a wall-to-wall forest ACD map of Sabah, also at 30 m resolution. We selected a deep learning model for this work after comparing outputs from gradient boosting regression, a random forest model, a generalized linear model (with and

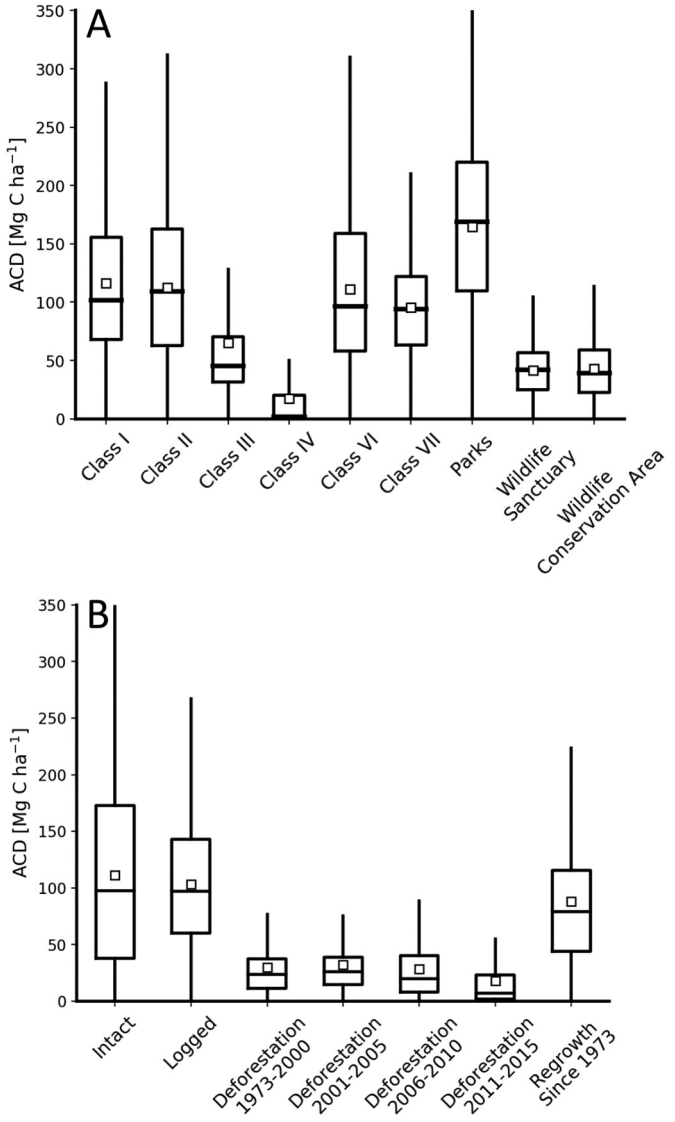

Fig. 2. (A) Aboveground carbon density (ACD) statistics throughout the State of Sabah sorted by forest management class (see Fig. A1). (B) ACD statistics by land cover classification of Gaveau et al. (2016). Red dots and lines are mean and median ACD values. Box plots indicate one standard deviation, and whiskers indicate data range.

without regularization penalties), and a support vector machine regression model. Deep learning models connect input features (here, the environmental data) to the response variable (the LiDAR ACD) through a sequence of layers of 'neurons.' With enough data, this modeling approach allows for the encapsulation of virtually any continuous underlying functional form, even those that may be complex and highly nonlinear in nature (Hastie et al., 2009). To create an upscaling model at high spatial resolution, each pixel was determined using all of the information in the data layers for that pixel as well as the data layers in surrounding pixels (illustrated in Fig. A9). This assisted in accounting for boundary effects inherent to the mapped data, and also allowed the model to build in features of the landscape only evident at the multi-pixel level.

Following tuning of model meta-parameters, we selected a five-layer neural network with four identical internal layers of 200 neurons each. We used a *softplus* activation function for each layer (Dugas et al., 2001), which is a smoothed version of the commonly used rectified linear unit (ReLU) activation. We used the mean absolute error as the loss function, solved with an Adam optimizer (Kingma and Ba, 2014). To account for the fact that the collected ACD distribution is heavily skewed towards the lower end of ACD, we weighted samples > 300 Mg C ha^{-1} at 5 times their original value, and samples between 200 and 300 Mg C ha^{-1} at twice their original value. We selected these thresholds by looking for models with the least bias under visual inspection of the ACD disparity under a 10-fold validation. All models were created using a Theano framework (Al-Rfou et al., 2016). Finally, we upscaled only the data coincident with all forests throughout Sabah with the exception of mangroves and timber plantations, as delineated by Sabah Forestry Department geographic information system maps.

2.6. Upscaling uncertainty

We estimated the uncertainty in our statewide ACD predictions using the methodology described by Asner et al. (2013). We used the error analysis from a 10-fold cross-validation to derive the mean absolute deviation as a function of the predicted ACD. We then applied a linear interpolation function derived from the cross-validation to the upscaled ACD map to estimate our mapping uncertainty throughout Sabah. We tested at both 30 m (0.09 ha) and 1.0 ha mapping resolutions (Fig. A10). In both cases, model precision was high (R^2 = 0.70–0.71), and errors were generally distributed in an even manner around the 1:1 line (low bias). Root mean squared error (RMSE) was 41.6 Mg C ha^{-1} at 30 m mapping resolution, diminishing to 34.1 Mg C ha^{-1} at 1.0 ha resolution, in accordance with published errors for LiDAR-based mapping of forest aboveground carbon density (Mascaro et al., 2011; Zolkos et al., 2013). When further tested with spatially explicit holdout sets, distributed randomly across a 20 by 20 grid overlaid on the data set, the RMSE of the 30 m mapping resolution increased by 2.5 Mg C ha^{-1} while the RMSE of the 1.0 ha mapping resolution decreased by 3.0 Mg C ha^{-1}, indicating that the model is transferable over distances equivalent to the gaps in the flight coverage.

2.7. Feature influence

To investigate how the deep-learning model responds to different environmental variables, we calculated the influence that each particular feature had on the model output. This was performed by iteratively withholding each feature and then estimating the modeled RMSE. Features that, when removed, result in a higher error relative to the base model are deemed to be more influential. The resulting error deviations from each iteration compared to the full data set were then scaled and normalized, with the results shown in Fig. A11. Relative elevation – a hydrological metric related to water and nutrient availability (Balzotti et al., 2016; Detto et al., 2013) – was the most important factor in scaling the CAO-based measurements to the Sabah scale. Additionally, shortwave-infrared reflectance, location, and elevation were important. All other factors had contributory roles.

3. Results and discussion

Results of the Sabah statewide mapping of forest ACD are shown in Fig. 1a, with an estimate of uncertainty provided in Fig. 1b. The mapping resolution is 30 m (0.09 ha), and the map excludes mangroves as well as oil palm and timber plantations. Uncertainties range from very low (approx. 15%) in areas of very high carbon stocks, to > 40% in areas of much lower carbon storage. Such relative errors are well documented in past research (Asner et al., 2014), with the highest carbon stocks displaying the lowest relative error.

A breakdown of forest carbon stocks based on the Sabah government's "Forest Class" system indicated that Sabah's fully protected "Parks" currently retain the highest carbon densities, averaging 165 Mg C ha^{-1} (Fig. 2a). Class I (protection) and Class II (commercial) contain nearly 50% lower ACD levels of about 100–110 Mg C ha^{-1}. Class VI (virgin jungle) and Class VII (wildlife) reserves retain even lower aboveground carbon densities of approximately 95 Mg C ha^{-1}. Notably, Class I, II, VI, and VII have prior logging histories (Gaveau

et al., 2014). Class III (domestic) and Class IV (amenity) forest designations are associated with much lower ACD levels, averaging just 45 and < 5 Mg C ha^{-1}, respectively. Other low-carbon density designations include Wildlife Sanctuaries and Wildlife Conservation Areas (Fig. 2a).

We also considered the mapped ACD results by forest history provided by Gaveau et al. (2016), which revealed three findings (Fig. 2b). First, forests mapped by Gaveau et al. (2016) as either intact or logged had statistically similar carbon stocks averaging about 100 Mg C ha^{-1}. This comparison is limited by the fact that "intact" forests encompass a wide range of conditions and forest protection histories, from previously logged forests to protected areas such as Maliau Basin with 220 ± 69 Mg C ha^{-1}, and Danum Valley with 207 ± 71 Mg C ha^{-1} (Table A1). Other "intact" forest reserves yielded even higher carbon densities, with Imbak Canyon producing the highest mean stock of 229 ± 81 Mg C ha^{-1}, and the highest mapped ACD hectare of forest occurred in Kinabalu Park at 500 Mg C ha^{-1} (Table A1).

The Gaveau et al. (2016) classification was also used to assess the effects of past deforestation. We found that landscapes deforested for oil palm or timber plantations contain areas of residual forest with average carbon densities of between 7 and 26 Mg C ha^{-1}, after masking out oil palm and timber plantation cover (Fig. 2b). Independent of time-since-clearing, these landscapes harbor small tracks of forest that could be useful for animal habitat and/or as a starting point for reforestation efforts. Two additional findings further support this notion. First, more recently deforested lands, cleared between 2011 and 2015 contain significantly lower forest carbon (7 Mg C ha^{-1}) compared to older deforested landscapes. Second, areas that Gaveau et al. (2016) mapped as having undergone regrowth since initial clearing prior to 1973 contain an average 80 Mg C ha^{-1}.

Using the Sabah-wide ACD map (Fig. 1a), we classified natural forests containing the top quartile and top 5% of carbon densities at 30 m resolution (Fig. 3). Particularly high carbon stocks were found in Class I and Park-designated land allocations, such as in the Crocker mountains, near Mount Kinabalu, Maliau Basin, Imbak Canyon, Danum Valley, Tawau Hills, and Tabin forest reserves (Fig. 3). While these reserves were expected to contain the highest carbon densities representing large tracts of remaining old growth, high-biodiversity forest, numerous areas of other high carbon stock forest were discovered in the State, particularly along the southern portion of Sabah, following the borders with Sarawak, Malaysia and Kalimantan, Indonesia. These areas remain relatively isolated today, compared to the rest of Sabah.

Additionally, 0.78 and 0.13 million ha of forests containing the top quartile and top 5% of mapped carbon stocks, respectively, were found outside of Class I or Park-designated reserves (Fig. 3), thus representing prime targets for new or improved forest protection. These areas alone contain about 151 Tg (million metric tons), or 38%, of State's total forest aboveground carbon that could be protected. High carbon stock forests such as these may or may not harbor high levels of biological diversity (Ashton and Hall, 1992; Sullivan et al., 2017). This possibility must be carefully tested and entered into the narrative on evaluating remaining forests for conservation. Additionally, we note that our results do not include belowground carbon storage, which may provide additional perspectives on the use of forests for carbon sequestration and other aspects deemed important for conservation and climate change mitigation.

We further assessed potential aboveground carbon storage gains in currently forested landscapes throughout Sabah. We compared the distribution of aboveground carbon stocks in all logged forests to those forests known to be free of past selective logging. The unlogged forests included a portion of Danum Valley, Imbak Canyon, and Maliau Basin, gazetted by Sabah state and verified by airborne LiDAR (Fig. 4). The results indicate that, as a whole, forests of Sabah have a highly skewed distribution of carbon stocks, with the most common carbon levels ranging from 20 to 120 Mg C ha^{-1} (Fig. 5a). In contrast, logging-free forests harbor much higher aboveground carbon stocks averaging 200 Mg C ha^{-1} (Fig. 5b), a value observed in ground-based studies (Slik et al., 2010; Sullivan et al., 2017). Although unlogged forests have a wide distribution of natural carbon densities, the difference in distributions clearly indicates that logged forests have a greatly suppressed amount of carbon stock above ground (Berry et al., 2010).

Building on these results, we estimate that if all current forests were to be protected and remain unlogged into the future, and if those protected forests were to accumulate carbon to meet the relative distribution of carbon stocks observed throughout unlogged forests today, the total amount of added aboveground carbon would be about 362.5 Tg (million metric tons) throughout Sabah. This value represents a near

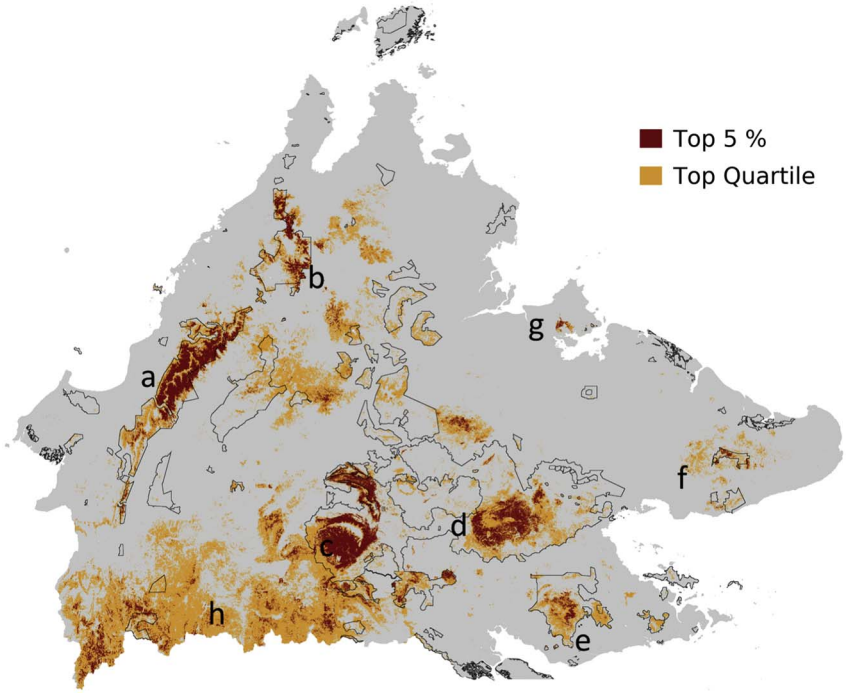

Fig. 3. Locations of the top 5% and top quartile of aboveground carbon densities (ACD) for natural forests of Sabah, Malaysia, not including mangroves. Thin black lines indicate the location of Sabah Forest "Class I" and "Parks" designated reserves, which are the most protected in the State. Lettering highlights areas of high carbon stock forest including (a) Crocker Range, (b) Mount Kinabalu area, (c) Maliau Basin and Imbak Canyon, (d) Danum Valley, (e) Tawau Hills area, (f) Tabin area, (g) Sepilok, and (h) southwestern Sabah near to the Sarawak, Malaysia and Kalimantan, Indonesian borders.

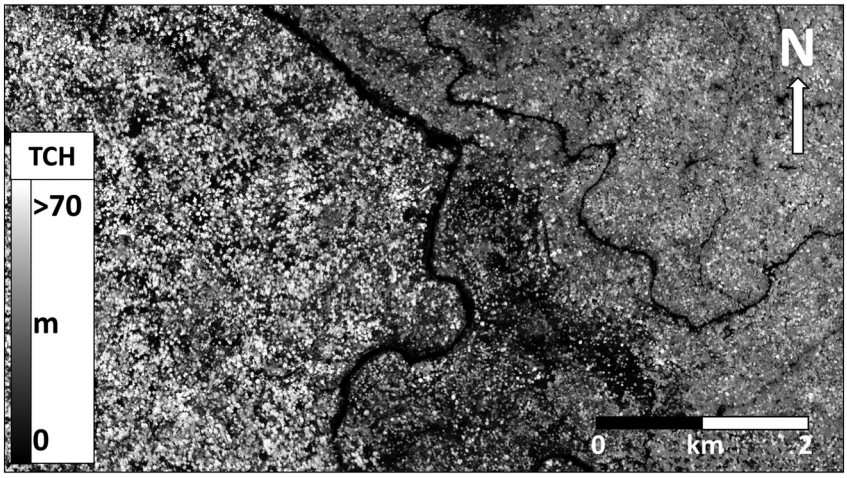

Fig. 4. Forest top-of-canopy height (TCH) where unlogged forest (left side of river) abuts a previously logged forest within Danum Valley, Sabah, Malaysia.

doubling of total forest carbon stored in Sabah's forests at present. Current and forthcoming protection depends upon forest management decisions ongoing within Sabah, but we can already detect the effect of environment on the recovery process (Fig. 6). Forests at higher elevation are much more likely to contain higher aboveground carbon stocks than lowland forests, an indicator that a lack of forest accessibility has facilitated post-logging regeneration (Meijaard et al., 2005).

Overall, our findings indicate that enormous amounts of carbon persist in both logged and unlogged forests throughout Sabah. Our estimated aboveground carbon densities of 150 + Mg C ha^{-1} in unlogged forest meet or exceed carbon stocks of most tropical forests, including much of the Amazon and Congo basins (Avitabile et al., 2016; Saatchi et al., 2011). Even the logged forests of Sabah currently harbor as much carbon per hectare as old growth forests of the western Amazon basin and other tropical forests worldwide (Asner et al., 2014; Poorter et al., 2016). Moreover, given that forests of Sabah occupy a relatively confined area of 3.6 million ha, most of which is lowland to sub-montane forest, the potential for recovery of carbon stocks can be assessed through comparison of the widespread logged and the much more limited areas of unlogged forest. Based on current distributions of forest carbon stocks, we contend that Sabah could, theoretically, double its total aboveground carbon stock just by allowing the current areas of logged forest to fully regenerate. Timescales of regeneration to full carbon density are poorly understood, but studies around the humid tropics suggest a century or more time will be needed (Keller et al., 2004; Pinard and Cropper, 2000; Sasaki et al., 2016).

Our results provide a critically important input into the process of identifying high conservation value forests, and to determine potential areas for new protections that conserve and recover Sabah's remaining forests. Forest carbon is one of several factors indicating the stature and

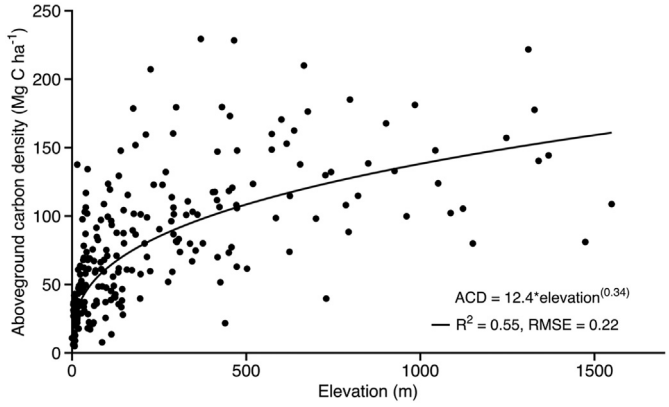

Fig. 6. Relationship between elevation and aboveground carbon density for the forest reserves listed in Table A1. Each dot represents one forest reserve.

intactness of tropical forests, including the identification of old growth trees and stands. Additional spatially-explicit information on biological diversity in the canopy, as well as among the animal and plant inhabitants of the forest, will be important factors needed to identify remaining forests for protection in Sabah and throughout other regions of Borneo and Southeast Asia. One way to combine the results from carbon and biodiversity mapping might involve a hierarchical approach, where high carbon stock forests are identified as we have done here, and then high biodiversity areas within those high carbon stock forests are delineated and used to prioritize areas for protection. The resulting prioritization will be developed using forthcoming maps of forest canopy functional diversity, derived using the approach outlined

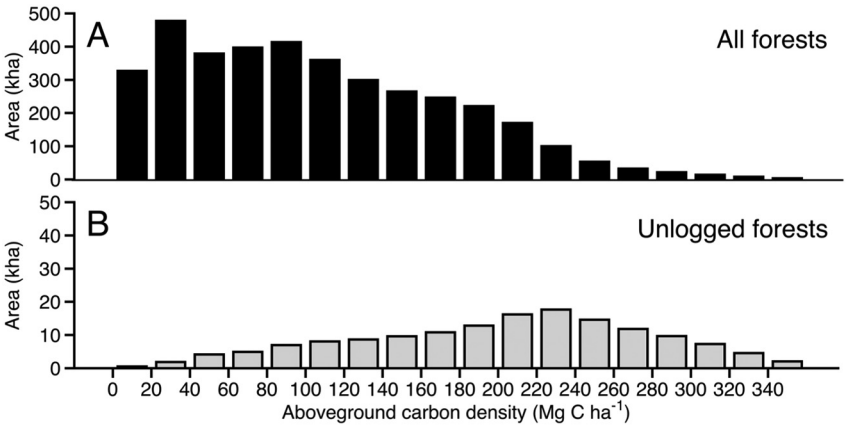

Fig. 5. (A) Distribution of aboveground carbon density (ACD) for natural forests throughout Sabah. (B) Distribution for unlogged natural forests only.

in Asner et al. (2017).

Acknowledgements

We thank three anonymous reviewers and the editor for suggestions and insights that greatly improved the manuscript. We thank our partners from the Sabah Forestry Department, LEAP, PACOS Trust, Layang Layang Aerospace, and other organizations within Malaysia for their support of this study. Airborne mapping, processing and analysis was funded by the UN Development Programme GEF, Avatar Alliance Foundation, Roundtable on Sustainable Palm Oil, Worldwide Fund for Nature, Morgan Family Foundation, and the Rainforest Trust. D.A. Coomes and T. Jucker were supported by NERC grant NE/K016377/1, and D.A. Coomes by an international academic fellowship from the Leverhulme Trust. The Carnegie Airborne Observatory has been made possible by grants and donations to G.P. Asner from the Avatar Alliance Foundation, Margaret A. Cargill Foundation, David and Lucile Packard Foundation, Gordon and Betty Moore Foundation, Grantham Foundation for the Protection of the Environment, W. M. Keck Foundation, John D. and Catherine T. MacArthur Foundation, Andrew Mellon Foundation, Mary Anne Nyburg Baker and G. Leonard Baker Jr., and William R. Hearst III.

Appendix A

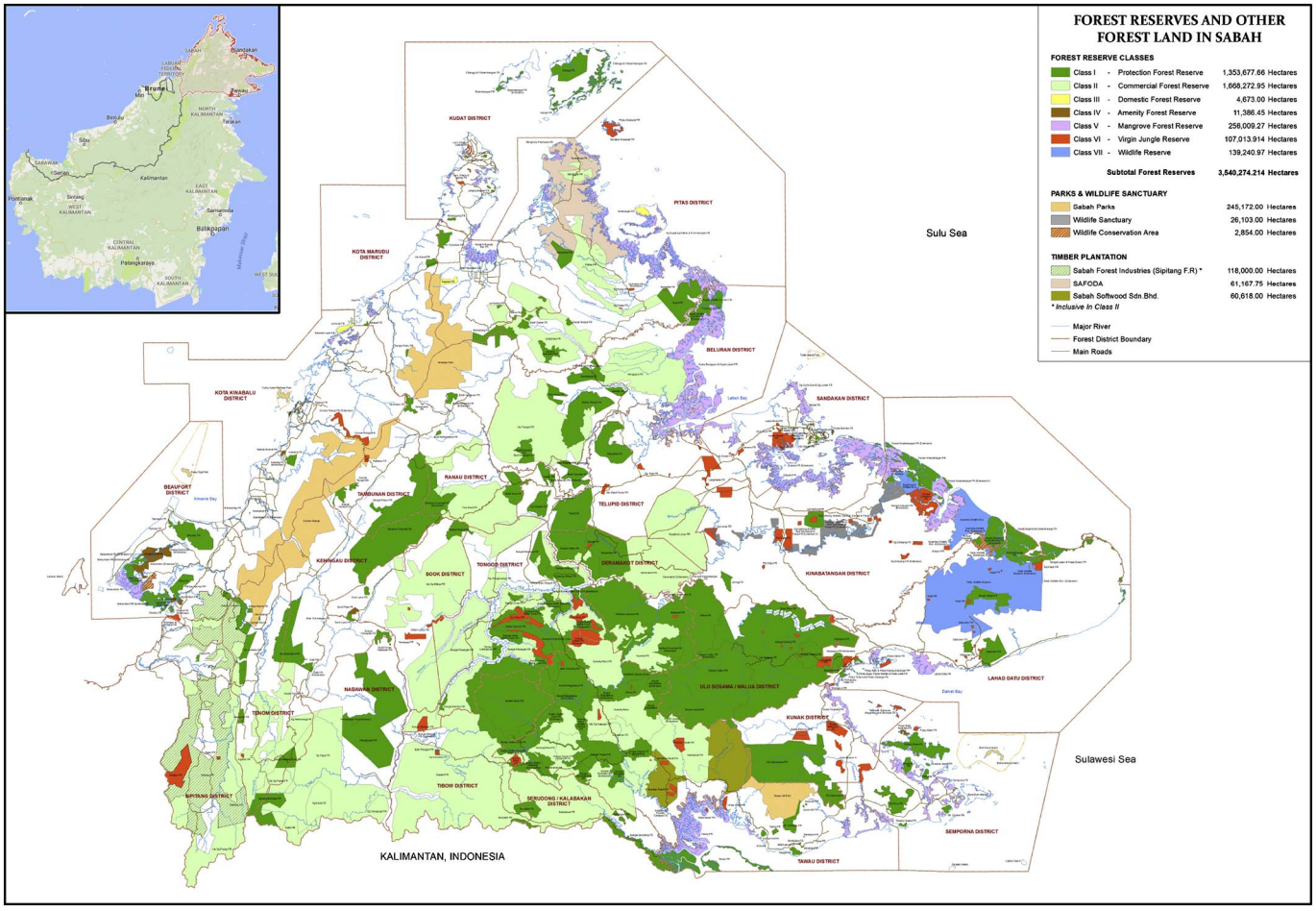

Fig. A1. Statewide distribution of official forest reserves and other forest lands throughout Sabah, Malaysia. Map courtesy of Sabah Forestry Department. Inset map shows the location of Sabah outlined in red on the island of Borneo.

Fig. A2. Distribution of data collection flightlines from the Carnegie Airborne Observatory sampling of Sabah. Each line is 1.5–3.0 km wide (swath). Areas of particularly concentrated mapping coincide with landscapes containing field calibration plots.

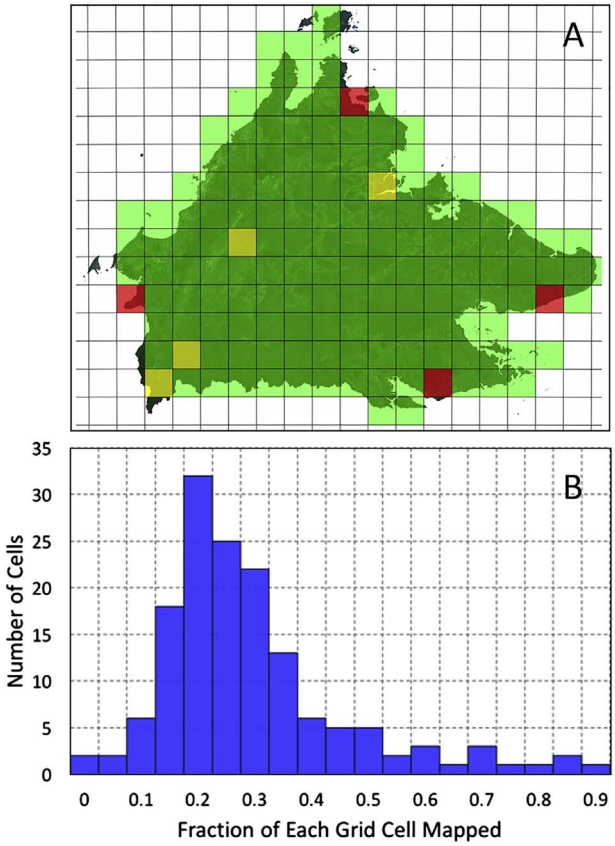

Fig. A3. (A) Resulting of near real-time modeling of Carnegie Airborne Observatory data density required to fully meet data sampling requirements. Green indicates 100% coverage, yellow indicates 95% coverage, and red indicates 90% coverage. Grid lines indicate mapping units of 25 km × 25 km. (B) The fraction each 25 km × 25 km grid cell mapping unit covered during CAO data collection flights. (For interpretation of the references to colour in this figure legend, the reader is referred to the web version of this article.)

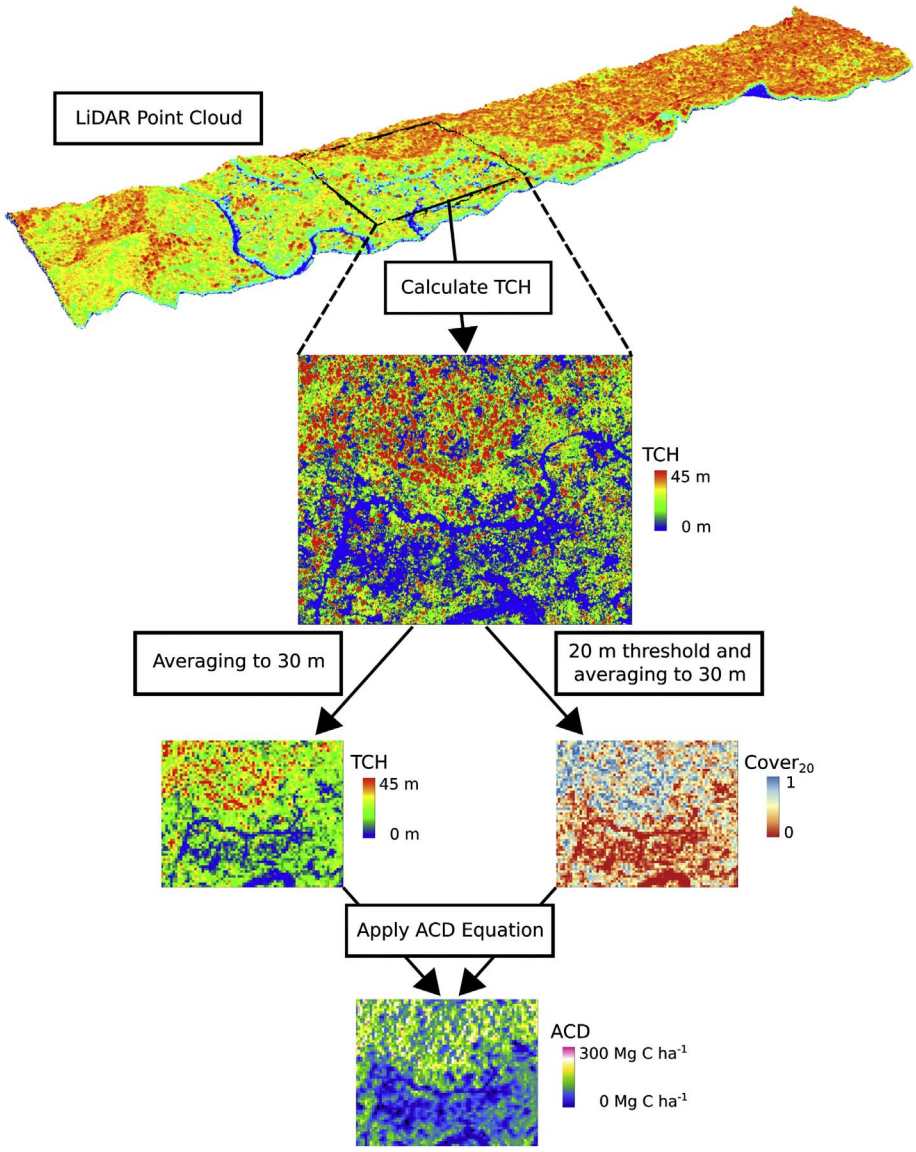

Fig. A4. Workflow illustrating how airborne LiDAR point cloud data are used to estimate aboveground carbon density (ACD). First, tree canopy height (TCH) is calculated from the point cloud at 2 m ground-level resolution. Next, TCH is averaged to 30 m resolution, and the fraction of 2 m TCH pixels that exceed 20 m is used to determine $Cover_{20}$ at 30 m resolution. Finally, we calculate aboveground carbon density (ACD) as a function of TCH and $Cover_{20}$ (see main text).

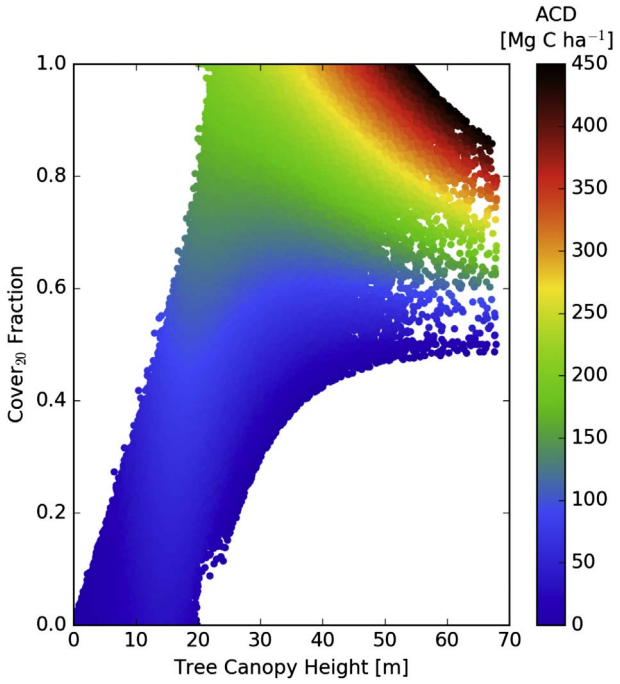

Fig. A5. Aboveground carbon density (ACD) as a function of top-of-canopy height (TCH) and the fraction of the canopy that exceeds 20 m (Cover$_{20}$) for all CAO flight data (see main text for equation).

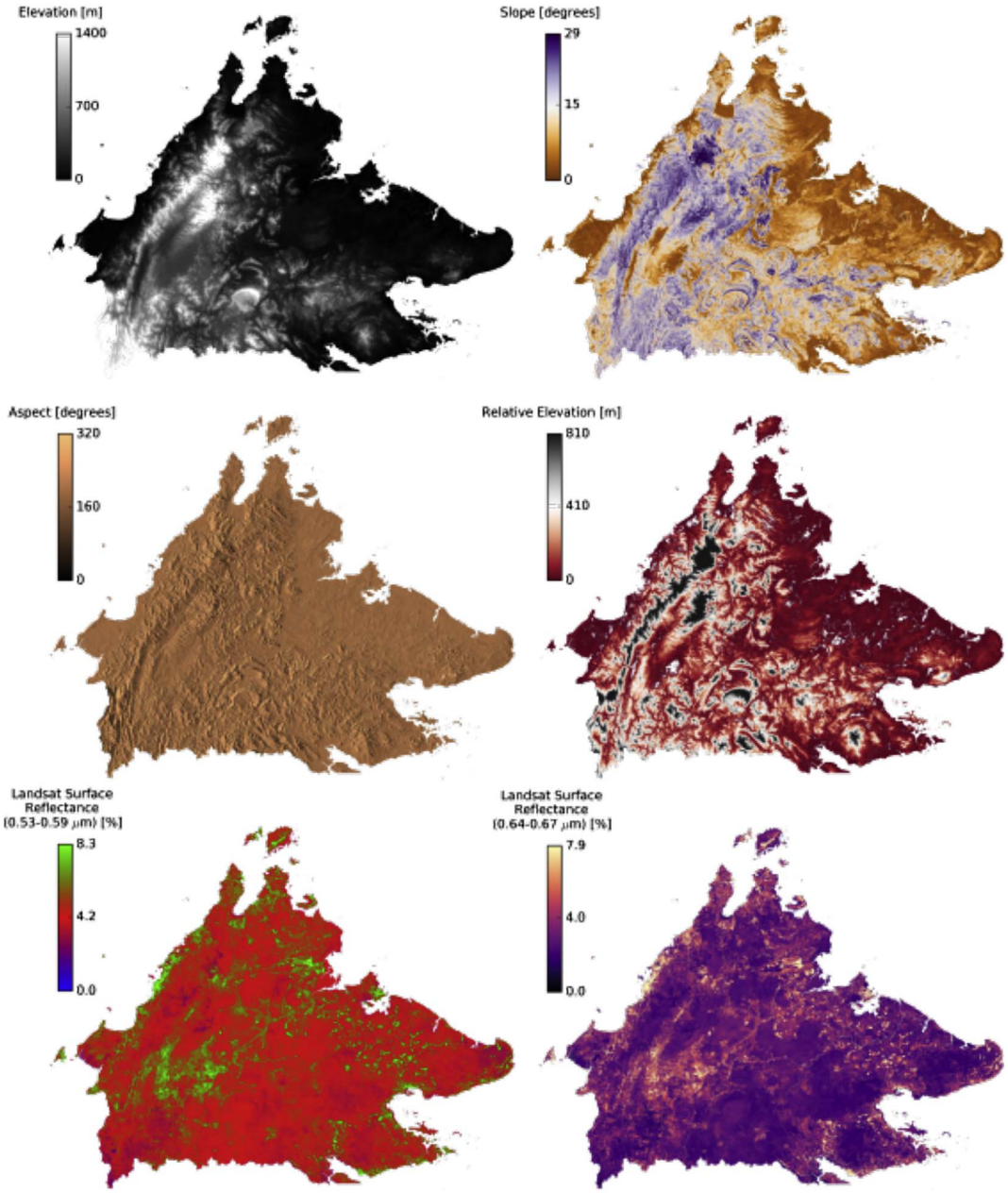

Fig. A6. Six of the environmental dataset layers used in upscaling airborne LiDAR to the Sabah level. Topographic elevation, slope, aspect, and relative elevation were derived from NASA SRTM data, and Landsat-8 surface reflectance data were composited between 15 Oct 2015 and 15 Oct 2016 to generate a cloud-free mosaic.

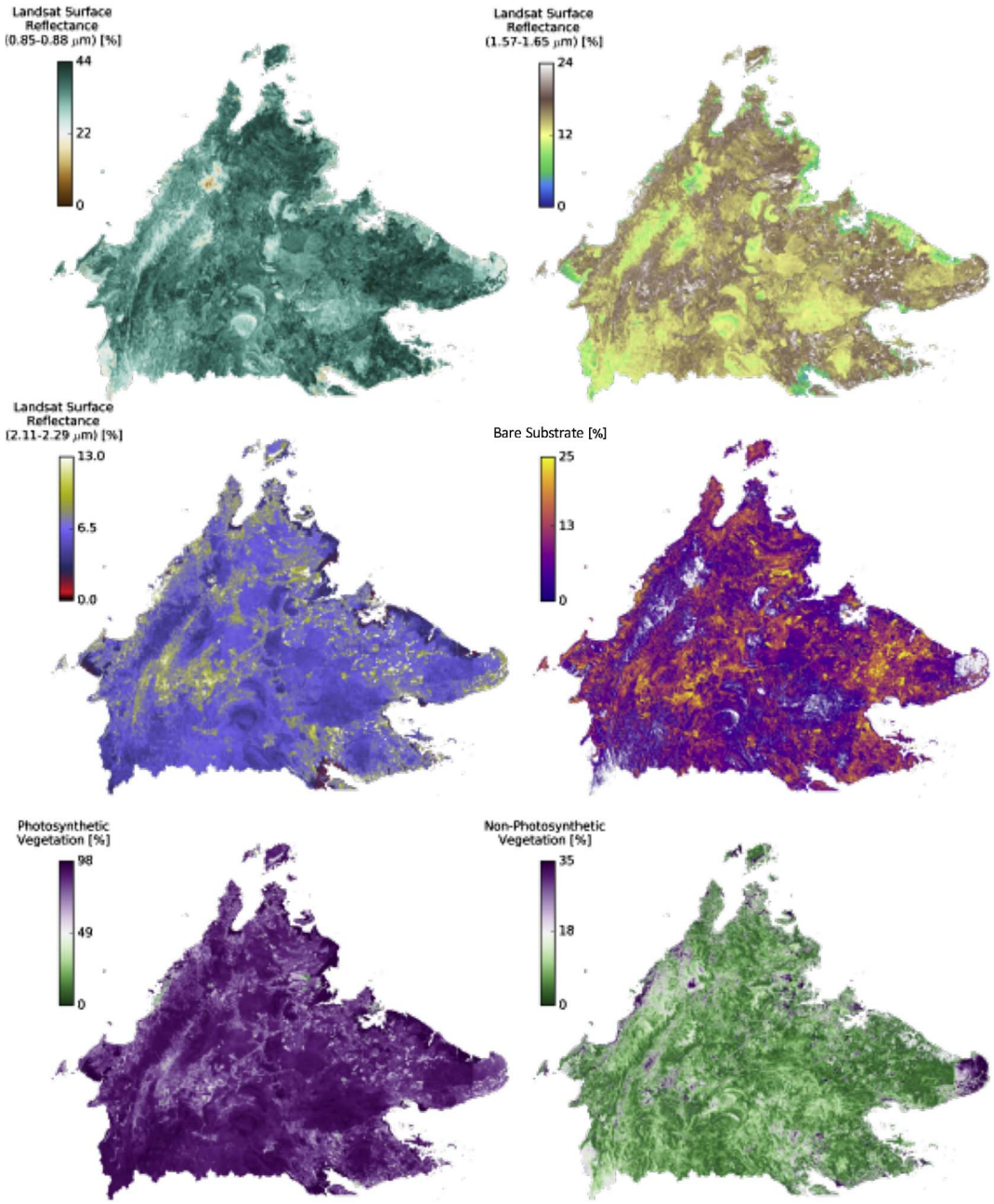

Fig. A7. Six of the environmental dataset layers used in upscaling airborne LiDAR to the Sabah level. Landsat-8 surface reflectance data were composited between 15 Oct 2015 and 15 Oct 2016 to generate a cloud-free mosaic. Bare substrate, photosynthetic, and non-photosynthetic vegetation were derived from Landsat-8 surface reflectance data.

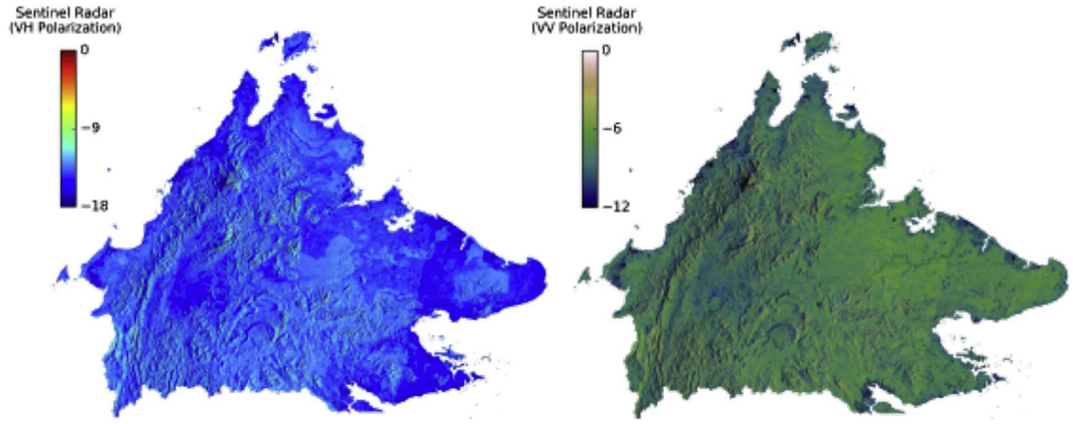

Fig. A8. Two of the environmental dataset layers used in upscaling airborne LiDAR to the Sabah level. Sentinel synthetic aperture radar (SAR) data with VH and VV polarizations were collected using the interferometric wide swath mode were aggregated between 1 Feb 2016 and 1 July 2016 using the per-pixel median to account for view-angle effects.

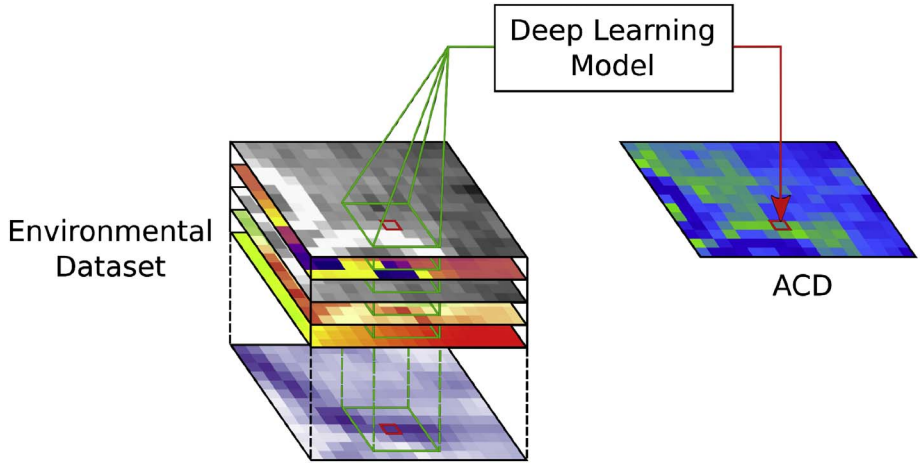

Fig. A9. Visualization of the deep learning model-based upscaling process. Data from each layer in the environmental dataset in a 5 × 5 pixel window (shown in green) around the target pixel (shown in red) are used in each model prediction. (For interpretation of the references to colour in this figure legend, the reader is referred to the web version of this article.)

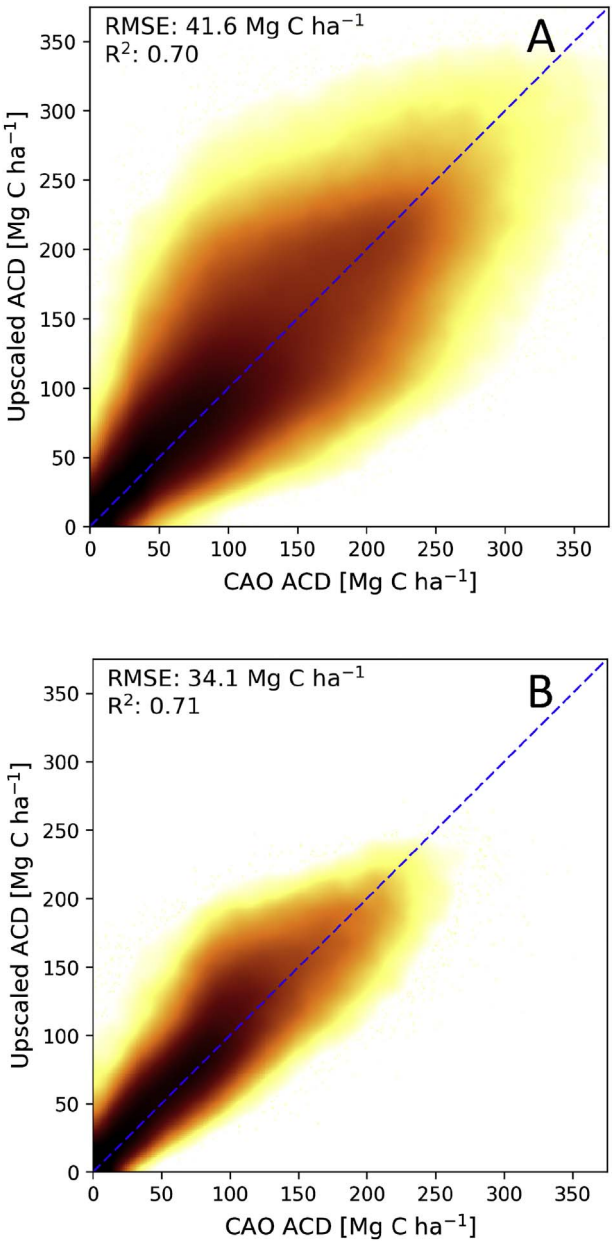

Fig. A10. Verification that ACD estimated from airborne LiDAR data are represented in the upscaled Sabah-wide ACD map. The deviation is shown for both the (A) 30 m resolution data and (B) one-hectare resolution. Both plots show minimal bias, and the hectare average shows reduced variation compared with the 30 m resolution predictions.

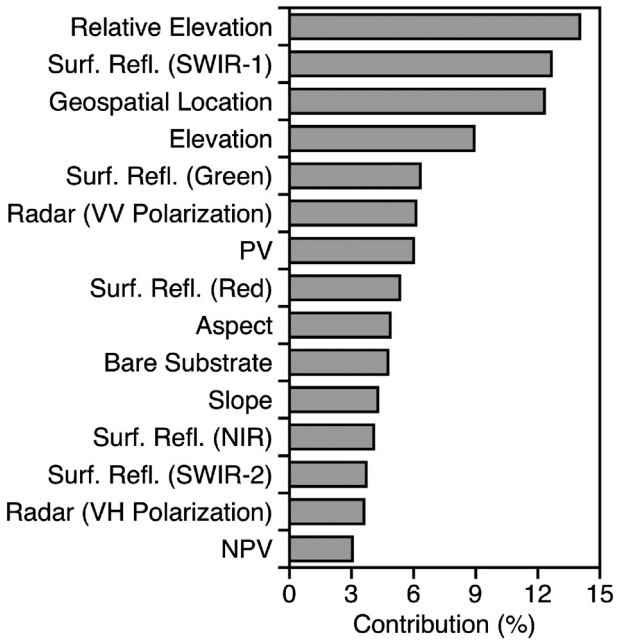

Fig. A11. The influence of each mapped environmental factor (Figs. A6–A8) on upscaling model performance. In order of contribution, the features are relative elevation, Landsat-8 surface reflectance (Surf. Refl.) from the SWIR-1 band, geospatial location, elevation, Landsat-8 surface reflectance from the green band, radar data in the VV polarization, photosynthetic vegetation (PV), Landsat-8 surface reflectance from the red band, aspect, bare substrate, slope, Landsat-8 surface reflectance from the NIR band, Landsat-8 surface reflectance from the SWIR-2 band, radar data in the VH polarization, and non-photosynthetic vegetation (NPV). (For interpretation of the references to colour in this figure legend, the reader is referred to the web version of this article.)

Table A1
Area, mean ± standard deviation of aboveground carbon density (ACD), 25th and 75th percentile ACD, and total standing aboveground carbon stock (AC) of each forest reserve in Sabah, Malaysia. Kha = thousands of hectares; Mg = megagrams or metric tons; Gg = gigagrams or thousand metric tons.

Forest reserve	Area (kha)	ACD (Mg C ha^{-1})	25th/75th percentile ACD (Mg C ha^{-1})	Total AC (Gg C)
Abai FR	1.27	28.31 ± 17.24	12.18/40.8	34.51
Agathis FR	0.20	185.16 ± 48.63	159.17/216.1	36.30
Apas FR	< 0.01	17.8 ± 9.19	11.56/23.29	0.09
Babanga FR	0.04	17.22 ± 7.54	11.88/22.73	0.72
Balat Damit Wildlife Rsv.	4.33	39.95 ± 26.55	26.74/45.84	172.65
Balat Damit Wildlife Rsv. (Ext.)	0.78	19.17 ± 22.55	2.7/31.69	14.86
Bald Hill FR	0.05	81.12 ± 49.7	41.78/114.23	4.26
Balembangan FR	0.36	28.77 ± 13.49	20.88/37.08	10.11
Banggi Island FR	10.90	63.44 ± 22.8	47.42/79.88	691.24
Baradaya FR	0.02	21.26 ± 4.55	17.97/23.93	0.42
Basio FR	0.22	167.75 ± 28.7	156.86/185.76	36.08
Batu Punggul FR	0.11	179.74 ± 75.36	119.6/238.17	20.59
Batu Timbang FR	0.26	147.86 ± 78.62	91.79/183.99	38.53
Batumapun FR	0.16	31.07 ± 8.91	27.93/36.4	4.47
Bengkoka FR	6.23	26.49 ± 10.94	19.5/33.3	164.97
Bengkoka Peninsula FR	11.05	22.73 ± 8.85	17.5/28.18	246.88
Bidu-Bidu FR	16.09	122.82 ± 38.56	97.74/150.71	1975.93
Binsuluk FR	12.17	22.51 ± 30.71	1.49/33.17	265.26
Bod Tai FR	0.25	69.56 ± 24.98	54.24/82.37	17.52
Bonggaya FR	61.42	22.27 ± 24.21	4.17/32.07	1367.42
Botitian FR	1.93	84.77 ± 36.52	58.76/108.79	163.41
Brantian-Tantulit FR	4.09	101.38 ± 61.9	49.79/145.88	414.29
Bukau Api-Api FR	0.90	37.2 ± 25.73	20.28/49.44	33.09
Bukit Balingkadus FR	0.30	80.04 ± 48.08	33.68/121.43	24.28
Bukit Hampuan FR	1.43	102.25 ± 73.3	35.77/150.61	144.92
Bukit Kuamas FR	7.38	71.48 ± 42.78	35.17/99.11	526.95
Bukit Kuamas FR (Ext.)	0.19	50.45 ± 29.65	28.19/71.43	9.59
Bukit Monkobo & Bukit Mentapok FR	5.44	138.47 ± 47.58	106.8/171.85	744.30
Bukit Pekan Nabawan FR	0.04	98.61 ± 54.64	54.85/141.09	4.16

Bukit Piton FR	11.66	42.75 ± 25.1	22.46/59.95	498.15
Bukit Taviu FR	8.63	147.07 ± 47.46	114.63/180.85	1269.19
Crocker Range FR	3.30	125.92 ± 65.16	71.09/177.72	415.22
Crocker Range FR (Ext.)	< 0.01	99.9 ± 66.59	44.62/142.21	0.60
Crocker Range National Park	140.05	180.82 ± 73.51	130.15/234.5	25,317.67
Dagat FR	0.16	103.13 ± 38.61	83.65/122.87	16.89
Dalit FR	1.95	63.03 ± 32.34	38.37/86.52	122.52
Danum Valley FR	43.51	207.36 ± 71.33	157.19/261.85	9021.11
Danum Valley FR (Ext.)	0.10	143.2 ± 34.1	116.18/169.66	14.55
Deramakot FR	55.06	134.77 ± 60.22	91.12/175.46	7419.86
Deramakot FR (Ext. I)	0.05	71.76 ± 47.08	35.77/96.69	3.82
Deramakot FR (Ext. II)	0.38	71.03 ± 30.84	51.72/83.37	27.10
Elopura FR	26.88	26.91 ± 12.84	20.51/31.74	706.90
Elopura FR (Ext.)	0.06	22.88 ± 11.15	15.39/29.89	1.34
Gana FR	0.88	88.44 ± 48.13	54.66/121.39	77.24
Ganui FR	0.32	83.24 ± 27.87	64.54/101.58	26.89
Garinono FR	0.45	61.47 ± 30.8	39.56/81.74	27.77
Gemok Hill FR	0.44	115.45 ± 69.46	63.23/152.97	50.43
Gn. Kumaka FR	5.15	157.15 ± 55.9	123.8/202.01	667.80
Gn. Lumaku FR	98.98	129.85 ± 71.51	69.19/187.85	6831.62
Gn. Lumaku FR	10.35	77.31 ± 63.87	29.92/110.66	731.42
Gn. Rara FR	5.12	70.16 ± 58.15	25.67/95.98	353.91
Gn. Rara Wildlife Corridor FR	0.05	70.75 ± 40.75	46.74/86.41	2.54
Gn. Tinkar FR	6.63	96.26 ± 37.69	72.84/116.72	512.09
Gomantong FR	11.54	69.19 ± 26.43	54.03/81.39	1809.84
Gum-Gum FR	10.00	52.57 ± 33.63	28.23/70.84	962.11
Imbak Canyon FR	17.02	228.35 ± 77.25	174.61/288.68	3886.74
Imbok FR	0.12	80.16 ± 42.43	48.51/104.63	10.01
Jembongan FR	1.58	30.57 ± 20.84	12.74/45.52	48.37
Kabili Sepilok FR	4.26	164.18 ± 76.06	96.58/224.42	699.44
Kabili Sepilok FR (Ext.)	0.01	31.43 ± 9.06	26.04/34.29	0.39
Kalabakan FR	181.99	70.05 ± 54.95	22.02/106.55	12,620.90
Kalumpang FR	3.75	101.28 ± 64.74	41.35/155.05	379.23
Karakit FR	0.03	22.45 ± 18.17	0.71/40.6	0.62
Kawag Gibong FR	0.73	100.92 ± 41.48	73.86/121.06	73.68
Kawang FR	1.59	81.6 ± 29.44	60.95/102.21	129.47
Kebun Cina FR	0.15	91.5 ± 60.22	46.47/125.01	13.86
Kelawat FR	0.20	57.55 ± 16.7	46.33/68.41	11.58
Kerangas FR	0.38	108.1 ± 64.83	51.22/159.63	40.94
Keruak FR	0.25	63.65 ± 20.28	52.07/76.82	15.83
Kg. Hindian FR	0.58	37.69 ± 20.07	26.67/43.89	21.89
Khazanah Sandakan Fd (Hq) FR	< 0.01	14.22 ± 11.63	4.32/24.05	0.12
Khazanah Sandakan Fd (Hq) FR (Ext.)	< 0.01	7 ± 7.3	0.98/12.69	0.02
Kinabalu Park	75.23	140.34 ± 81.42	73.74/201.96	10,535.27
Kitabu FR	0.12	48.47 ± 10.32	42.67/55.37	5.92
Klias FR	3.65	97.66 ± 45.81	73.25/122.52	356.91
Kretam FR	0.42	75.71 ± 34.52	61.42/95.87	31.85
Kuala Bonggaya & Kuala Labuk FR	52.67	34.83 ± 13.84	28.73/40.04	1806.90
Kuala Bonggaya & Kuala Labuk FR (Ext.)	0.03	49.3 ± 26.25	33.44/63.57	1.33
Kuala Segama & Kuala Meruap FR	22.56	30.38 ± 13.36	23.22/35.87	667.97
Kuala Tingkayu FR	4.44	28.63 ± 13.06	20.11/38.35	123.26
Kuala Tomani FR	17.95	98.21 ± 44.79	66.5/132.34	1761.91
Kuamut FR	46.97	85.34 ± 44.52	56.36/108.89	4006.68
Kudat & Marudu Bay FR	10.03	29.73 ± 11.84	24.01/36.03	294.05
Kudat & Marudu Bay FR (Ext. I)	0.58	32.37 ± 12.03	25.59/40.23	14.75
Kudat & Marudu Bay FR (Ext. II)	0.01	25.39 ± 5.89	22.81/28.97	0.23
Kukusan FR	0.07	18.51 ± 17.44	1.48/32.45	1.17
Kulamba Wildlife Rsv.	20.35	41.72 ± 29.74	21.5/56.88	844.10
Kulamba Wildlife Rsv. (Ext.)	0.26	63.4 ± 26.27	47.78/80.74	16.42
Kungkular FR	1.27	39.68 ± 30.86	19.34/49.78	49.96
Labuan FR	0.19	36.16 ± 7.73	31.26/41.16	6.97
Labuk Road FR	0.12	101.88 ± 72.46	50.28/136.74	12.18
Lahad Datu FR	8.73	26.97 ± 11.31	21.11/33.42	223.03
Lahad Datu FR (Ext.)	0.05	34.61 ± 14.31	24.53/45.37	1.54
Lajong FR	0.28	40.88 ± 9.4	34.82/46.97	11.40
Lamag FR	2.13	99.06 ± 48.55	64.55/128.36	211.15

Leila FR	0.29	93.55 ± 57.35	49.95/137.57	27.46
Lema'as FR	1.45	40.63 ± 12.73	34.47/48.02	58.13
Limau-Limauan FR	0.22	35.63 ± 9.28	29.84/40.67	7.95
Lingkabau FR	71.47	123.54 ± 52.67	85.69/160.45	8828.80
Lipaso FR	3.53	79.95 ± 43.62	46.27/107.36	282.14
Loro FR	0.52	38.69 ± 10.63	33.87/45.39	20.16
Lungmanis FR	6.75	69.03 ± 30.73	46.38/89.68	465.60
Lungmanis FR (Ext.)	< 0.01	37.11 ± 20.44	19.6/53.1	0.26
Madai-Baturong FR	5.85	71.09 ± 40.78	44.28/92.04	415.72
Malawaring FR	0.09	5.55 ± 6.69	0.91/7.23	0.51
Maliau Basin FR	58.29	220.37 ± 69.32	190.11/263.84	12,834.08
Maliau Buffer Zone FR	46.64	144.13 ± 68.47	90.57/187.08	6719.30
Maliau Buffer Zone FR (Ext. I)	5.18	132.67 ± 51.75	95.94/167.41	686.76
Maliau Buffer Zone FR (Ext. II)	13.80	136.81 ± 55.96	98.62/174.69	1886.26
Maligan FR	9.24	108.76 ± 54.45	58.52/158.09	1000.83
Malua FR	33.94	101.69 ± 44.82	72.7/123.17	3451.06
Malubuk FR	0.22	123.59 ± 44.85	91.73/146.7	27.51
Mamahat FR	0.08	36.6 ± 7.9	31.86/41.8	2.82
Mandahan FR	< 0.01	26.29 ± 2.62	24.87/27.62	0.19
Mandahan FR (Ext.)	< 0.01	52.65 ± 14.84	43.47/61.75	0.01
Mandamai FR	5.34	86.78 ± 24.82	71.26/101.28	462.98
Marine Parks	0.02	14.73 ± 13.93	2.6/21.98	0.10
Materis FR	0.26	68.03 ± 28.93	49.84/87.06	17.72
Matunggong FR	0.35	51.9 ± 14.95	42.26/60.4	18.36
Meliau Range FR	22.92	106.66 ± 35.87	81.57/131.71	2444.66
Membalua FR	0.07	45.17 ± 27.47	28.91/53.66	3.26
Mengilan FR	6.59	123.92 ± 47.32	87.47/159.18	814.30
Menumbok FR	5.68	36.82 ± 15.49	29.02/44.75	202.70
Menumbok FR (Ext. I)	6.04	32.35 ± 8.13	30.29/36.82	208.08
Menumbok FR (Ext. II)	2.00	34.9 ± 12.33	27.75/41.69	63.45
Menumbok FR (Ext. III)	0.54	35.75 ± 9.04	33.6/39.34	19.01
Merisuli FR	0.56	37.12 ± 17.91	23.76/48.53	20.90
Mile 16 Keningau FR	< 0.01	21.75 ± 38.64	0.39/21.09	0.20
Milian-Labau FR	2.81	117.52 ± 75.38	45.82/176.71	329.95
Milli Nonum FR	< 0.01	34.49 ± 20.93	21.43/40.62	0.21
Mt. Andrassy FR	8.68	110.78 ± 52.93	77.29/149.64	1317.93
Mt. Cochrane FR	55.04	51.62 ± 20.33	39.41/64.01	8973.59
Mt. Conner	1.79	38.29 ± 40.93	12.44/49.02	137.84
Mt. Hatton FR	48.58	151.85 ± 70.7	98.85/197.42	4234.56
Mt. Louisa FR	7.05	163.05 ± 65.06	114.78/213.85	577.90
Mt. Louisa FR (Ext.)	7.74	77.55 ± 42.52	48.6/105.94	950.97
Mt. Magdalena FR	3.59	87.24 ± 43.73	61.55/107.54	397.79
Mt. Magdalena FR (Ext.)	2.92	81.96 ± 34.23	64.37/98.26	149.98
Mt. Mandalom FR	0.78	73.95 ± 31.42	50.31/95.52	26.61
Mt. Pock FR	19.39	122.9 ± 46.57	96.59/154.31	1433.61
Mt. Walker FR	0.15	104.29 ± 47.96	65.61/135.79	15.74
Mt. Wullersdorf FR	8.08	132.2 ± 66.78	89.13/182.34	1064.38
Nabahan FR	0.35	44.83 ± 12.08	36.91/51.35	15.76
Nabahan FR (Ext.)	0.13	27.84 ± 8.72	23.46/34.28	1.08
Northern Gunung Rara FR	8.44	73.31 ± 43.24	41.72/97.74	617.00
Northern Kuamut FR	69.42	76.69 ± 37.51	55.31/91.3	5322.93
Nuluhon Trusmadi FR	78.68	105.45 ± 46.63	71.48/135.36	8292.47
Nurod-Urod FR	1.65	210 ± 39.88	188.72/235.36	346.75
P. Baik & P. Kalung-Kalungan FR	0.55	57.9 ± 30.02	30.21/83.31	30.91
P. Banggi & P. Balambangan FR	0.29	27 ± 10.7	20.62/33.62	15.06
P. Batik Kulambu FR	0.82	58.89 ± 29.42	35.62/80.15	48.14
P. Bohaydulong	0.02	55.72 ± 30.61	30.77/78.91	0.06
P. Gaya	< 0.01	61.81 ± 33.97	36/84.81	0.04
P. Miaga	0.02	4.99 ± 5.97	0.19/8.49	0.64
P. saga P. Saddle & P. Laila FR	0.03	44.76 ± 33.67	18.59/62.68	1.19
P. Silingan	8.72	12.8 ± 11.69	2.01/20.95	226.89
P. Sipadan	0.08	10.86 ± 2.61	8.88/13.7	1.88
P. Tetagan	0.02	33.66 ± 17.79	22.33/45.65	0.03
Pababag FR	0.87	8.94 ± 8.1	1.42/15.03	6.91
Padas Damit FR	7.49	9.5 ± 13.9	0.39/14.31	57.81
Padas Damit FR (Ext.)	0.28	13.13 ± 12.75	1.92/21.92	3.71

Paitan FR	41.72	59.38 ± 26.22	40.72/77.88	2476.92
Pangi FR	0.42	73.79 ± 23.57	60.34/85.18	30.90
Pekan Baru Tongod FR	< 0.01	7.78 ± 6.02	2.28/11.26	0.05
Pekan Telupid FR	0.03	13.61 ± 15.91	1.01/23.61	0.46
Pensiangan FR	68.46	114.85 ± 33.98	92.71/137.47	7862.07
Pin-Supu FR	4.67	47.35 ± 25	28.94/63.26	221.02
Pulau Batik FR	0.35	61.27 ± 31.27	38.34/84.25	20.37
Pulau Berhala FR	0.19	67.25 ± 40.79	38.63/91.75	11.32
Pulau Malawali FR	0.79	23.79 ± 10.34	17.72/29.45	10.91
Pulau Sakar FR	0.75	60.35 ± 26.06	39.53/78.92	43.83
Pulau Tambun & Pulau Saranga FR	0.02	29 ± 9.6	22.65/34.14	0.29
Quoin Hill FR	0.06	118.35 ± 72.49	45.5/181.37	6.59
Rafflesia FR	0.56	221.78 ± 49.2	203.89/251.33	124.43
Rumbia FR	< 0.01	8.02 ± 7.32	1.73/14.99	0.02
Rumbia FR (Ext.)	< 0.01	2.35 ± 0.66	1.99/2.6	0.00
Sapagaya FR	0.70	79.9 ± 30.36	60.4/100.38	55.84
Sapagaya FR (Ext.)	2.50	92.38 ± 41.71	62.57/116.8	230.84
Sapulut FR	231.72	160.02 ± 49.38	131.27/195.81	37,059.99
Segaliud Lokan FR	57.29	75.29 ± 34.83	50.82/97.96	4313.46
Segarong FR	2.00	48.63 ± 41.86	20.81/68.37	96.75
Selangan Island FR	0.16	19.52 ± 9.57	14.23/26.33	1.20
Sempilor Malawali FR	2.47	28.37 ± 15.49	19.39/39.78	65.11
Semporna FR	18.07	21.12 ± 11.49	14.14/27.75	316.86
Sepagaya FR	4.06	80.05 ± 46.71	50.41/101.22	325.06
Sepilok FR	1.13	36.96 ± 17.46	26.57/42.67	41.08
Sg. Anjeranjermut FR	3.85	173.16 ± 57.6	139.21/214.38	667.11
Sg. Gologob FR	8.32	31.7 ± 17.09	25.39/34.02	263.58
Sg. Gum-Gum & Sg. Loboh FR	19.51	30.87 ± 21.5	20.83/33.92	2286.41
Sg. Imbak Buffer Zone FR	18.27	117.21 ± 75.59	64.95/153.14	1600.97
Sg. Imbak Buffer Zone FR (Ext.)	18.07	87.66 ± 39.51	64.25/103.75	2915.07
Sg. Imbak FR	4.65	161.42 ± 66.61	113.9/208.36	421.86
Sg. Imbak FR (Ext.)	14.20	90.72 ± 44.73	59.16/116.34	2503.97
Sg. Kabu FR	1.23	176.39 ± 24.28	164.28/191.94	143.83
Sg. Kapur FR	< 0.01	116.9 ± 46.52	87.34/143.47	0.22
Sg. Kinabatangan FR	29.06	26.78 ± 10.14	18.23/34.04	1167.82
Sg. Kinabatangan Valley	3.86	40.36 ± 23.75	23.24/56.06	107.20
Sg. Lasun & Pulau Evans FR	1.84	28.24 ± 14.51	23.57/36.09	124.88
Sg. Lokan FR	8.33	67.98 ± 28.29	49.66/83.62	387.59
Sg. Mangkuwagu FR	6.45	46.57 ± 24.67	29.28/64.26	241.81
Sg. Maruap FR	0.13	37.54 ± 14.43	29.27/43.65	8.45
Sg. Paitan FR	0.13	64.58 ± 23.51	45.13/83.68	7.22
Sg. Paitan FR (Ext.)	123.49	57.01 ± 14.4	45.9/67.44	9237.94
Sg. Pinangah FR	7.70	74.84 ± 49.16	40.28/99.71	514.25
Sg. Radapan FR	7.73	67.01 ± 39.2	32.96/93.42	1401.21
Sg. Salilir FR	0.34	181.28 ± 39.47	160.95/209.02	77.58
Sg. Sansiang FR	0.60	229.43 ± 82.31	167.36/297.43	37.61
Sg. *Sap*i FR	8.65	62.32 ± 38.96	29.86/87.37	827.34
Sg. Serudong FR	0.03	99.59 ± 40.88	77.03/128.09	4.08
Sg. Siliawan (Ext. I)	0.02	144.33 ± 49.98	110.95/176.91	1.83
Sg. Siliawan (Ext. II)	2.15	119.44 ± 46.67	86.69/153.56	343.99
Sg. Siliawan FR	1.16	160.04 ± 36.53	135.22/183.94	67.55
Sg. Simpang FR	0.09	58.37 ± 31.41	36.07/78.47	4.17
Sg. Simpang FR (Ext.)	4.24	44.94 ± 25.95	24.69/63.91	288.33
Sg. Sugut Sg. Paitan & Jembongan FR	105.75	27.66 ± 12.24	20.81/33.68	17,183.93
Sg. Sugut Sg. Paitan & Jembongan FR (Ext.)	20.58	22.36 ± 13.42	13.06/32.29	1859.44
Sg. Sumagas FR	14.41	68.05 ± 45.38	35.26/98.34	1915.38
Sg. Tagul FR	10.30	162.52 ± 41.82	138.06/193.02	1573.43
Sg. Talibu FR	19.85	90.42 ± 34.45	68.26/112.2	2980.10
Sg. Telekosang FR	7.01	132.92 ± 33.83	110.61/157.19	987.70
Sg. Temalasak FR	4.78	152.91 ± 33.8	130.35/176.09	547.88
Sg. Tiagau FR	2.72	150.11 ± 60.73	103.12/198.55	82.85
Sg. Tiagau FR (Ext.)	31.75	141.04 ± 89.53	49.23/219.37	865.96
Sg. Tongod FR	0.14	114.73 ± 42.95	84.27/145.31	2.85
Siaungau & Mesapol FR	0.84	47.69 ± 34.62	19.44/70.26	39.25
Sibuga FR	0.01	29.45 ± 20.12	14.86/39.97	0.35
Sibyte FR	2.30	39.42 ± 22.35	23.77/54.12	89.69

Silabukan FR	11.31	101.11 ± 45.51	71.36/128.57	1142.25
Silam FR	0.35	38 ± 29.8	17.17/54.31	12.90
Silimpopon FR	1.91	73.81 ± 27.43	53.46/94.48	140.62
Sipitang FR	250.47	99.88 ± 63.02	47.04/154	24,784.72
Sitompok FR	0.51	43.38 ± 27.76	17.45/63.7	22.06
Sook Lake FR	1.38	33.95 ± 19.55	18.78/46.99	46.79
Sook Plain FR	0.76	50.18 ± 30.57	30.18/66.78	37.90
Sosopodon FR	0.01	81.14 ± 53.09	28.94/126.56	0.84
Sugut FR	23.31	33.97 ± 18.64	21.14/46.19	791.09
Sugut Wildlife Corridor FR	0.30	47.26 ± 18.98	36.25/59.33	14.05
Sulaman Lake FR	2.20	30.21 ± 12.42	25.66/38.42	65.84
Sungai Katambalang FR	5.31	147.94 ± 35.01	129.14/172.51	785.05
Sungai Kiluyu FR	0.98	108.05 ± 33.18	87.59/131.01	105.44
Sungai Lulungoyan FR	2.14	59.25 ± 24.69	44.77/73.28	126.69
Sungai Penawan FR	2.25	137.76 ± 56.91	91/183.99	309.79
Sungai Segama FR	0.78	21.17 ± 18.54	4.83/33.7	16.49
Sungai Taliwas FR	9.57	113.79 ± 48.03	79.25/144.6	1088.24
Tabawan Bohayan Maganting & Silumpat Islands FR	0.99	66.28 ± 29.23	45.92/88.3	60.84
Tabin FR	0.41	135.18 ± 59.32	94.35/165.82	54.93
Tabin Wildlife Rsv.	111.80	106.36 ± 45.29	78.99/128.67	11,888.55
Tabin Wildlife Rsv. (Ext.)	0.27	62.54 ± 33.96	36.01/87.71	16.82
Tagaroh FR	1.57	120.74 ± 68.64	58.43/175.7	189.19
Tajong FR	0.43	129.41 ± 83.13	63.89/184.49	56.06
Tamalang FR	0.11	49 ± 7.44	44.48/53.95	5.18
Taman Botanikal Sepilok FR	0.10	78.33 ± 66.55	27.26/113.05	8.16
Taman Pulau Tiga	0.73	49.56 ± 17.39	42.52/57.13	34.11
Taman Tunku Abdul Rahman	1.23	96.5 ± 48.31	59.53/132.68	106.00
Tambalugu FR	0.19	22.16 ± 8.26	15.52/29.15	4.25
Tambulanan FR	3.26	170.6 ± 49.98	139.49/204.82	555.94
Tamparuli FR	0.06	60.49 ± 23.41	47.04/76.97	3.66
Tangkulap FR	27.26	97.2 ± 32.51	79.1/115.09	2649.39
Tanjong Nagas FR	0.36	60.87 ± 36.23	29.5/90.82	21.80
Tanjung Tumunong Hallo FR	0.02	18.06 ± 16.72	5.5/24.98	0.62
Tatahan FR	22.68	33.47 ± 15.31	19.8/45.58	2659.70
Tawai FR	37.48	117.67 ± 51.41	80.41/157.35	965.96
Tawau FR	0.53	26.65 ± 14.73	16.6/36.27	6.04
Tawau FR (Ext.)	28.03	12.29 ± 12.07	2.31/21.56	4380.05
Tawau Hills Park	< 0.01	156.25 ± 52.1	123.25/194.85	0.25
Teak Plantation FR	0.01	25.74 ± 10.33	21.55/32.44	0.01
Tegaipil Island	1.94	6.13 ± 4.02	2.32/9.51	279.60
Tenompok FR	0.59	144.33 ± 55.8	110.27/187.14	10.43
Timbah FR	0.29	108.76 ± 36.76	90.83/130.87	31.85
Timbun Mata FR	11.44	58.98 ± 39.32	25.45/86.04	671.45
Timimbang FR	11.45	87.96 ± 35.95	66.99/105.63	1007.10
Timimbang FR (Ext.)	0.06	60.1 ± 23.29	45.8/77.29	3.53
Tinagat FR	1.01	27.91 ± 12.72	19.42/34.27	28.10
Trusan Kinabatangan FR	38.25	31.21 ± 15.8	23.86/34.38	1183.82
Trusan Kinabatangan FR (Ext.)	3.89	31.51 ± 22.52	15.46/43.56	111.77
Trusan Sugut FR	8.53	48.99 ± 23.21	31.6/64.33	411.28
Trusmadi FR	97.07	132.18 ± 51.75	96.78/170.51	12,829.33
Ulu Dusun Agricultural FR	0.10	87.06 ± 25.34	73.18/103.1	8.64
Ulu Kalumpang FR	50.91	103.13 ± 66.8	47.93/153.97	5247.25
Ulu Kukut FR	1.30	59.74 ± 24.94	44.09/75.52	77.39
Ulu Sapa Payau FR	0.72	87.53 ± 43.06	66.84/109.45	63.13
Ulu Segama FR	127.19	106.25 ± 54.02	70.01/136.43	13,503.73
Ulu Sg. Milian	77.71	61.58 ± 49.12	17.61/98.58	4771.19
Ulu Sg. Napagon FR	0.52	148.56 ± 59.95	103.81/190.6	77.96
Ulu Sg. Padas FR	43.59	177.67 ± 41.07	152.7/207.42	7728.80
Ulu Telupid FR	6.35	105.81 ± 43.78	79.31/135.68	671.92
Ulu Tungud FR	94.91	111.68 ± 51.9	78.92/142.91	10,598.41
Umas-Umas FR	0.83	25.56 ± 17.62	15.09/31.77	21.27
Weston FR	0.30	25.4 ± 9.49	20.97/31.91	5.38
Wildlife Conservation Area	4.85	34.73 ± 23.79	18.14/44.72	168.25

References

Al-Rfou, R., Alain, G., Almahairi, A., Angermueller, C., Bahdanau, D., Ballas, N., Bastien, F., Bayer, J., Belikov, A., Belopolsky, A., 2016. Theano: A Python Framework for Fast Computation of Mathematical Expressions. (arXiv preprint arXiv:1605.02688).

Ashton, P.S., Hall, P., 1992. Comparisons of structure among mixed dipterocarp forests of north-western Borneo. J. Ecol. 459–481.

Asner, G.P., Mascaro, J., 2014. Mapping tropical forest carbon: calibrating plot estimates to a simple LiDAR metric. Remote Sens. Environ. 140, 614–624.

Asner, G.P., Knapp, D.E., Balaji, A., Paez-Acosta, G., 2009. Automated mapping of tropical deforestation and forest degradation: CLASlite. J. Appl. Remote. Sens. 3, 033543.

Asner, G., Clark, J., Mascaro, J., Vaudry, R., Chadwick, K.D., Vieilledent, G., Rasamoelina, M., Balaji, A., Kennedy-Bowdoin, T., Maatoug, L., Colgan, M., Knapp, D., 2012a. Human and environmental controls over aboveground carbon storage in Madagascar. Carbon Balance Manag. 7, 2.

Asner, G.P., Knapp, D.E., Boardman, J., Green, R.O., Kennedy-Bowdoin, T., Eastwood, M., Martin, R.E., Anderson, C., Field, C.B., 2012b. Carnegie airborne observatory-2: increasing science data dimensionality via high-fidelity multi-sensor fusion. Remote Sens. Environ. 124, 454–465.

Asner, G., Mascaro, J., Anderson, C., Knapp, D., Martin, R., Kennedy-Bowdoin, T., van Breugel, M., Davies, S., Hall, J., Muller-Landau, H., Potvin, C., Sousa, W., Wright, J., Bermingham, E., 2013. High-fidelity national carbon mapping for resource management and REDD+. Carbon Balance Manag. 8, 7.

Asner, G.P., Knapp, D.E., Martin, R.E., Tupayachi, R., Anderson, C.B., Mascaro, J., Sinca, F., Chadwick, K.D., Higgins, M., Farfan, W., 2014. Targeted carbon conservation at national scales with high-resolution monitoring. Proc. Natl. Acad. Sci. 111, E5016–E5022.

Asner, G., Martin, R., Knapp, D., Tupayachi, R., Anderson, C., Sinca, F., Vaughn, N., Llactayo, W., 2017. Laser-guided imaging spectroscopy to map forest traits and guide conservation. Science 355, 385–389.

Avitabile, V., Herold, M., Heuvelink, G., Lewis, S.L., Phillips, O.L., Asner, G.P., Armston, J., Ashton, P.S., Banin, L., Bayol, N., 2016. An integrated pan-tropical biomass map using multiple reference datasets. Glob. Chang. Biol. 22, 1406–1420.

Balzotti, C.S., Asner, G.P., Taylor, P.G., Cole, R., Osborne, B.B., Cleveland, C.C., Porder, S., Townsend, A.R., 2016. Topographic distributions of emergent trees in tropical forests of the Osa Peninsula, Costa Rica. Ecography 40, 829–839.

Berry, N.J., Phillips, O.L., Lewis, S.L., Hill, J.K., Edwards, D.P., Tawatao, N.B., Ahmad, N., Magintan, D., Khen, C.V., Maryati, M., 2010. The high value of logged tropical forests: lessons from northern Borneo. Biodivers. Conserv. 19, 985–997.

Breiman, L., 2001. Random forests. Mach. Learn. 45, 5–32.

Brown, S., Lugo, A.E., 1982. The storage and production of organic matter in tropical forests and their role in the global carbon cycle. Biotropica 14, 161–187.

Bryan, J.E., Shearman, P.L., Asner, G.P., Knapp, D.E., Aoro, G., Lokes, B., 2013. Extreme differences in forest degradation in Borneo: comparing practices in Sarawak, Sabah, and Brunei. PLoS One 8, e69679.

Coomes, D.A., Dalponte, M., Jucker, T., Asner, G.P., Banin, L.F., Burslem, D.F.R.P., Lewis, S.L., Nilus, R., Phillips, O.L., Phua, M.-H., 2017. Area-based vs tree-centric approaches to mapping forest carbon in Southeast Asian forests from airborne laser scanning data. Remote Sens. Environ. 194, 77–88.

Detto, M., Muller-Landau, H.C., Mascaro, J., Asner, G.P., 2013. Hydrological networks and associated topographic variation as templates for the spatial organization of tropical forest vegetation. PLoS One 8, e76296.

Dugas, C., Bengio, Y., Bélisle, F., Nadeau, C., Garcia, R., 2001. Incorporating second-order functional knowledge for better option pricing. Adv. Neural Inf. Proces. Syst. 472–478.

Gaveau, D.L.A., Sloan, S., Molidena, E., Yaen, H., Sheil, D., Abram, N.K., Ancrenaz, M., Nasi, R., Quinones, M., Wielaard, N., 2014. Four decades of forest persistence, clearance and logging on Borneo. PLoS One 9, e101654.

Gaveau, D.L.A., Sheil, D., Husnayaen, M.A.S., Arjasakusuma, S., Ancrenaz, M., Pacheco, P., Meijaard, E., 2016. Rapid conversions and avoided deforestation: examining four decades of industrial plantation expansion in Borneo. Sci Rep 6.

Google, 2015. Google Earth Engine: A Planetary-scale Geo-spatial Analysis Platform.

Hastie, T., Tibshirani, R., Friedman, J., 2009. The Elements of Statistical Learning, 2nd edition. Springer, New York.

Houghton, R.A., 2000. Interannual variability in the global carbon cycle. J. Geophys. Res.-Atmos. 105, 20121–20130.

Jomo, K.S., Chang, Y.T., Khoo, K.J., 2004. Deforesting Malaysia: The Political Economy and Social Ecology of Agricultural Expansion and Commercial Logging. Zed Books.

Jucker, T., Asner, G., Dalponte, M., Brodrick, P., Philipson, C., Vaughn, N., Brelsford, C., Burslem, D., Deere, N., Ewers, R., Kvasnica, J., Lewis, S., Malhi, Y., Milne, S., Nilus, R., Pfeifer, M., Phillips, O., Qie, L., Renneboog, N., Reynods, G., Riutta, T., Struebig, M., Svátek, M., Teh, Y., Turner, E., Coomes, D., 2017. A regional model for estimating the aboveground carbon density of Borneo's tropical forests from airborne laser scanning. Remote Sens. Environ (paper in review).

Kasischke, E.S., Christensen Jr., N.L., Stocks, B.J., 1995. Fire, global warming, and the carbon balance of boreal forests. Ecol. Appl. 5, 437–451.

Keller, M., Asner, G.P., Silva, N., Palace, M., 2004. Sustainability of selective logging of upland forests in the Brazilian Amazon: carbon budgets and remote sensing as tools for evaluating logging effects. In: Zarin, D.J., Alavalapati, J.R.R., Putz, F.E., Schmink, M. (Eds.), Working Forests in the Neotropics: Conservation Through Sustainable Management? Columbia University Press, New York, pp. 41–63.

Kingma, D., Ba, J., 2014. Adam: A Method for Stochastic Optimization. (arXiv preprint arXiv:1412.6980).

Lindenmayer, D.B., Laurance, W.F., Franklin, J.F., Likens, G.E., Banks, S.C., Blanchard, W., Gibbons, P., Ikin, K., Blair, D., McBurney, L., Manning, A.D., Stein, J.A.R., 2013. New policies for old trees: averting a global crisis in a keystone ecological structure. Conserv. Lett. 7, 61–69.

Mascaro, J., Detto, M., Asner, G.P., Muller-Landau, H.C., 2011. Evaluating uncertainty in mapping forest carbon with airborne LiDAR. Remote Sens. Environ. 115, 3770–3774.

Masek, J.G., Vermote, E.F., Saleous, N.E., Wolfe, R., Hall, F.G., Huemmrich, K.F., Gao, F., Kutler, J., Lim, T.-K., 2006. A Landsat surface reflectance dataset for North America, 1990–2000. IEEE Geosci. Remote Sens. Lett. 3, 68–72.

Meijaard, E., Sheil, D., Nasi, R., Augeri, D., Rosenbaum, B., Iskandar, D., Setyawati, T., Lammertink, M., Rachmatika, I., Wong, A., 2005. Life after Logging: Reconciling Wildlife Conservation and Production Forestry in Indonesian Borneo. Cifor.

Pinard, M.A., Cropper, W.P., 2000. Simulated effects of logging on carbon storage in dipterocarp forest. J. Appl. Ecol. 37, 267–283.

Pinard, M., Howlett, B., Davidson, D., 1996. Site conditions limit pioneer tree recruitment after logging of dipterocarp forests in Sabah, Malaysia. Biotropica 28, 2–12.

Poorter, L., Bongers, F., Aide, T.M., Zambrano, A.M.A., Balvanera, P., Becknell, J.M., Boukili, V., Brancalion, P.H.S., Broadbent, E.N., Chazdon, R.L., 2016. Biomass resilience of Neotropical secondary forests. Nature 530, 211–214.

Réjou-Méchain, M., Tanguy, A., Piponiot, C., Chave, J., Hérault, B., 2017. Biomass: an r package for estimating above-ground biomass and its uncertainty in tropical forests. Methods Ecol. Evol. 8, 1163–1167.

Saatchi, S.S., Harris, N.L., Brown, S., Lefsky, M., Mitchard, E.T.A., Salas, W., Zutta, B.R., Buermann, W., Lewis, S.L., Hagen, S., Petrova, S., White, L., Silman, M., Morel, A., 2011. Benchmark map of forest carbon stocks in tropical regions across three continents. Proc. Natl. Acad. Sci. 108, 9899–9904.

Sasaki, N., Asner, G.P., Pan, Y., Knorr, W., Durst, P.B., Ma, H.O., Abe, I., Lowe, A.J., Koh, L.P., Putz, F.E., 2016. Sustainable management of tropical forests can reduce carbon emissions and stabilize timber production. Front. Environ. Sci. 4.

Slik, J.W.F., Aiba, S.I., Brearley, F.Q., Cannon, C.H., Forshed, O., Kitayama, K., Nagamasu, H., Nilus, R., Payne, J., Paoli, G., 2010. Environmental correlates of tree biomass, basal area, wood specific gravity and stem density gradients in Borneo's tropical forests. Glob. Ecol. Biogeogr. 19, 50–60.

Smith, J., Mulongoy, K., Persson, R., Sayer, J., 2000. Harnessing carbon markets for tropical forest conservation: towards a more realistic assessment. Environ. Conserv. 27, 300–311.

Sullivan, M.J.P., Talbot, J., Lewis, S.L., Phillips, O.L., Qie, L., Begne, S.K., Chave, J., Cuni-Sanchez, A., Hubau, W., Lopez-Gonzalez, G., 2017. Diversity and carbon storage across the tropical forest biome. Sci Rep 7, 39102.

UNFCCC, 2009. Methodological giudance for activities relating to reducing emissions from deforestation and forest degradation and the role of conservation, sustainable management of forests and enhancement of forest carbon stocks in developing countries. In: CU.N.F.C. o. C. Change (Ed.), Decision 4/CP.15. UNFCCC, Copenhagen, Denmark.

Zolkos, S.G., Goetz, S.J., Dubayah, R., 2013. A meta-analysis of terrestrial aboveground biomass estimation using lidar remote sensing. Remote Sens. Environ. 128, 289–298.